

# Investigating the Structure-Activity Relationship of Laulimalides Marine Macrolides as Promising Inhibitors for SARS-CoV-2 Main Protease (Mpro)

Alaa M. Elgohary,<sup>1</sup> Abdo A. Elfiky,<sup>1\*</sup> Florbela Pereira<sup>2</sup>, Mariam I. Gamal El-Din<sup>3,4</sup>, Mohamed A. Tammam<sup>5</sup>, Mohamed Sebak<sup>6</sup>, Sherif I. Hamdallah<sup>7,8</sup>, Emad Shehata<sup>4,9</sup> and Amr El-Demerdash<sup>10,11\*</sup>

<sup>1</sup>Department of Biophysics, Faculty of Sciences, Cairo University, Giza 12613, Egypt

<sup>2</sup>LAQV-REQUIMTE, Department of Chemistry, NOVA School of Science and Technology, Universidade Nova de Lisboa, 2829-516 Caparica, Portugal

<sup>3</sup>Department of Pharmacognosy, Faculty of Pharmacy, Ain-Shams University, 11566, Cairo, Egypt

<sup>4</sup>Quadram Institute Bioscience, Norwich Research Park, Norwich, Norfolk NR4 7UQ, UK

<sup>5</sup>Department of Biochemistry, Faculty of Agriculture, Fayoum University, Fayoum 63514, Egypt

<sup>6</sup>Microbiology and Immunology Department, Faculty of Pharmacy, Beni-Suef University, Beni-Suef 62514, Egypt

<sup>7</sup>School of Pharmacy, University of East Anglia, Norwich NR4 7TJ, UK

<sup>8</sup>Department of Pharmaceutics, Faculty of Pharmacy, Alexandria University, Alexandria, Egypt

<sup>9</sup>Chemistry of Flavour and Aroma Dept, National Research Centre, 33 El Buhouth St, Giza, 12622, Dokki, Egypt

<sup>10</sup>Division of Organic Chemistry, Department of Chemistry, Faculty of Sciences, Mansoura University, Mansoura 35516, Egypt

<sup>11</sup>Department of Biochemistry and Metabolism, the John Innes Centre, Norwich Research Park, Norwich NR4 7UH, UK

\*Correspondences:

[dr\\_abdo@cu.edu.eg](mailto:dr_abdo@cu.edu.eg), (Abdo A. Elfiky). Tel: +20 1003260523

[Amr.El-Demerdash@jic.ac.uk](mailto:Amr.El-Demerdash@jic.ac.uk) (Amr El-Demerdash) +44 7834240424

**Abbreviations:**

**ADME:** Absorption, distribution, metabolism, and excretion

**COVID-19:** Coronavirus disease 2019

**SARS-CoV-2:** severe acute respiratory syndrome-coronavirus 2

**MDMs:** Marine Derived Macrolides

**LMM:** Lantimalides Marine Macrolides

**MNPs:** Marine Natural Products

**MPro:** Main Protease

**MD:** Molecular Dynamics

**SARs:** Structure-Activity Relationships

**VMD:** Visual Molecular Dynamics

**RMSD:** Root Mean Square Deviation

**RMSF:** Root Mean Square Fluctuation

**MM-GBSA:** Molecular Mechanics-Generalized Born Surface Area

**SASA:** Solvent Accessible Surface Area

**Highlights:**

- Marine natural compounds are powerful natural leads against SARS-CoV-2 Mpro.
- Laulimalides are a distinctive class of 20-membered marine macrolides with prominent biomedical potentialities.
- Intensive virtual screening supported with SARs studies highlighted the laulimalides marine derived macrolides (**LMM**), particularly laulimalides LA4 (**6**) and LA18 (**13**) as potential antiviral hits for paving SARS-CoV-2 main protease.

**Keywords:**

SARS-CoV-2; virtual screening; molecular docking; molecular dynamics simulation; marine natural product, laulimalides marine macrolides

## Abstract

SARS-CoV-2, the new coronavirus variant is a world-wide health crisis. Over spans of human history, preparations derived from natural products have always been recognized as a preliminary source of medications. Taking into account the SARS-CoV-2 main protease (Mpro) as the essential element of the viral cycle and as a main target, herein we highlight a computer-aided comprehensive virtual screening for a focused chemical list of 14 laulimalides marine macrolides against SARS-CoV-2 main protease (Mpro) using a set of integrated modern computational techniques including molecular docking (MDock), molecule dynamic simulations (MDS) and structure-activity relationships (SARs) as well. Indeed, computational studies had disclosed two promising macrolides [laulimalides LA4 (**6**) and LA18 (**13**)] based on their remarkable ligand-protein energy scores and relevant binding affinities with the SARS-CoV-2 (Mpro) pocket residues. Consequentially, the two compounds were further investigated thermodynamically though deciphering their MD simulations at 100 ns, where they showed noticeable stability within the accommodated (Mpro) pockets. Moreover, in-deep SARs studies suggested the crucial roles of the C-23 substituted side chain and the C-20 methoxy as essential pharmacophoric structural features for activity. Such interesting outcomes are highly recommending further *in vitro/vivo* examinations regarding those marine macrolides and open a gate towards developing more effective antivirals drug leads.

## **1. Introduction**

The last few years have witnessed a breakthrough spread of the new coronavirus, SARS-CoV-2 (COVID-19), correlated with human respiratory disease (Zhou et al., 2023). The first case of the disease was initially identified in Wuhan, China in December 2019 (Zheng et al., 2020). The symptoms were characterized by a peculiar resistant pneumonia associated with elevated temperature, exhaustion, dry cough and occasional gastrointestinal symptoms (Alimohamadi et al., 2020).

The pandemic with its multiple variants swiftly invaded the world infecting more than 750 million individual and causing deaths which exceeded 6 million cases according to the recent WHO dashboard (Pan et al., 2023; W.H.O., 2023). Not only vulnerable individuals are susceptible to the infection and its consequences during the pandemic, but cases of frequent infections of vaccinated and pre-infected individuals still being reported (Tan et al., 2023). Hence, an imperative urgency arises for tremendous efforts to be directed towards discovering and developing of medicinal countermeasures to this pandemic virus including effective prophylactic vaccines and medical treatments (Ng et al., 2022).

Nature has been considered as a valuable treasure for drug discovery since antiquity (El-Din & Youssef; Ghareeb et al., 2020). Intriguingly, natural products are always regarded as a backbone of traditional medicinal systems used throughout the whole world (El-Din et al., 2023). Distinguished by their unique boundless structural diversity, natural sources are endlessly inspiring for their mining for novel bioactive chemical entities (Alimohamadi et al., 2020).

Natural terrestrial plants, despite being a rich source of secondary metabolites and a major fundamental provenance for traditional folk medicine over thousands of years, their overuse made them susceptible for overharvesting, depletion and extinction of many rare species of high medicinal value (Uzma et al., 2019). On the contrary, oceans and seas covering extensive areas of the planet exceeding 70 % of the earth's surface, represent a renewable as well as a sustainable source of bioactive natural products (Cheng & Mishra, 2022).

Besides, the marine environment, with its higher salinity, pressure and lower temperature compared to normal conditions of the terrestrial life, provoke distinctive adaptive metabolic mechanisms by the surrounding marine microorganisms ending in the production of a wide variety of natural products of significant pharmacological activities (Ma et al., 2016). Hence, the marine environment and its associated microorganisms have

recently received a remarkably growing attention for discovering an enormous scaffold diversity of natural products of medicinal importance (Carroll et al., 2022).

Marine macrolides, are considered among the distinctive classes of marine natural products that have lately been regarded as a fascinating mine for drug discovery (Das et al., 2022).

Pharmacologically, they demonstrated prominent biological activities including antibacterial, antifungal, anti-inflammatory, cytotoxic and antiviral potentials (Mooberry et al., 2004; Qi & Ma, 2011; Zhang et al., 2021). Macrolides, are being biosynthesized via the polyketide pathway, are characterized by their large macrocyclic lactone ring that is usually 14-, 15-, or 16-membered. Moreover, further 20-, 24-, 26- or 36-membered macrolides were also identified like oligomycin A and amphotericin B. Numerous patterns of alkylation, dehydration and oxygenation, through the polyene backbone accounts for the great chemical diversity among marine macrolides (Zhang et al., 2021).

Laulimalides are a distinctive class of 20-membered marine macrolides which were initially isolated from the marine chocolate sponge, *Cacospongia mycofijiensis* (Clark et al., 2006). Laulimalide (also known as fijianolide) has been reported as a prominent microtubule-stabilizing agent that significantly enhances the density of interphase microtubules, elicits the generation of abnormal mitotic spindles and microtubule bundles (Mooberry et al., 2004; Mooberry et al., 1999).

Indeed, it intensively inhibits cancer cell proliferation with notable potency against paclitaxel-resistant cells. It is also proved to possess another privilege; its superior capability of overcoming multidrug resistance emerging from P-glycoprotein (Churchill et al., 2016; Liu et al., 2007). Structurally, the laulimalide skeleton is characterized by its two dihydropyran rings (C5-C9) and (C23-C27), attached to the macrolide skeleton via 2,6-*trans* attachment and terminal *trans*-allylic alcohol attachment, respectively. It is also distinguished by the 2,3-*cis* unsaturated double bond, the presence of nine chiral centres at positions 5*R*, 9*S*, 11*S*, 15*R*, 16*S*, 17*S*, 19*S*, 20*S*, and 23*S* respectively and the *trans*-disubstituted epoxide at position C-16 and C-17 (Qi & Ma, 2011).

Nevertheless, laulimalide under mild acidic conditions undergoes ring opening of the fragile C16-C17-epoxide via the nucleophilic attack of the C-20 hydroxyl group generating the less potent isomer, isolaulimalide (Wender et al., 2008). Owing to the potent activities of laulimalide and its distinguished chemical structure, multiple research groups have worked on its total synthesis and the synthesis of various analogues in the

attempt of enhancing its stability and bioactivity especially under acidic conditions (Gollner & Mulzer, 2008; Wender et al., 2003). Besides, structurally simplified analogues of laulimalide were designed to reduce the cost of synthetic steps.

The groups of Ghosh, Paterson, and Mulzer accomplished the total chemical synthesis of laulimalide and a number of modified analogues (Ghosh & Wang, 2000; Mulzer & Öhler, 2003; Paterson et al., 2001). The elimination of C16-C17-epoxide and alkylation of C-20 hydroxyl group were among the strategies adopted in the synthesis of different laulimalide analogues including LA1 (**3**), LA2 (**4**), LA3 (**5**) and LA4 (**6**) (Mooberry et al., 2004). Besides, the conversion of the C2-C3-enoate to an alkynoate evidenced in the synthesis of LA3 was an effective way to alter the orientation of the C16-C17-epoxide relative to the C20-hydroxyl.

Moreover, analogues combining the two functional group conversions were also synthesized as LA4 (**6**) and LA5 (**7**) (Wender et al., 2003). Other function-oriented synthetic studies were accomplished to investigate the effect of altering the side chain substitution attached at C-22 on the antiproliferative effectiveness of the laulimalide. The importance of the alkene  $\pi$ -system inside the chain attached at C-22 in the antiproliferative effectiveness of the laulimalide was concluded from the diminished antiproliferative activity of the LA13 (**8**) analogue associated with the methyl ether attachment instead of the pyran unit.

Besides, diminished antiproliferative potency was demonstrated with the analogues, LA14 (**9**) and LA16 (**11**) with the pyran ring substituted by cyclohexane and aryl ring respectively. Meanwhile, epoxidized C21-C22 olefin, in LA15 (**10**), the minor side product in the synthesis of LA14 (**9**) did not show better potency than LA14 (**9**). However, the C-23-cyclohexane analogues, LA18 (**13**) and LA18` (**14**) with the unsaturated side chain demonstrated unpredicted enhanced potency (Mooberry et al., 1999). In the meantime, the significant impact of computational and bioinformatics tools has been conceded in the field of drug discovery (Romano & Tatonetti, 2019).

Applying computer science for characterizing and understanding the chemical behaviour and molecular attributes of specific chemical molecules has been recognized as the first crucial step in the track of discovering new lead compounds (El-Demerdash, Hassan, et al., 2021; Gamal El-Din et al., 2022; Gamal El-Din et al., 2018). By using various computational and bioinformatics tools, drug-protein interactions, the pharmacokinetics,

the stability, as well as the toxicity of a plenty of bioactive marine natural products including laulimalides would be easier to be estimated and elucidated (Amr et al., 2020; Hassan et al., 2021).

Thus, core bridgeheads between biological effectiveness and quantitative structure activity relationships could be consequently established (Alaa M Elgohary et al., 2022; Pereira et al., 2022). In this study, we comprehensively explore virtually a concise library of fourteen laulimalides marine-containing macrolides against SARS-CoV-2 main protease (Mpro) dimer using state-of-the-art of integrated computational tools including molecular docking, molecular dynamics (MD) simulations, binding free energy and SARs.

These *in-silico* methods successfully predicted novel potential inhibitors against Mpro and other drug targets of SARS-CoV-2 (Almutairi et al., 2022; Elfiky et al., 2022; Alaa M. Elgohary et al., 2022; Gomha et al., 2022; Ibrahim et al., 2022; Moriou et al., 2021). Continuing our ongoing strategy for identifying potential bioactive lead compounds derived from marine natural products (El-Demerdash et al., 2019; El-Demerdash et al.; El-Demerdash, Metwaly, et al., 2021; El-Demerdash et al., 2020; Tammam et al., 2023), herein we investigate the antiviral potentialities of 14 laulimalide-containing macrolides (LMM) utilizing comprehensive virtual screening against SARS-CoV-2 main protease (Mpro).

## **2. Materials and Methods**

### **2.1 Ligand structures preparation**

SCIGRESS 3.0 software was utilized to draw and minimize the structures of laulimalides (**1-14**) (Elfiky et al., 2016; Summers et al., 2012). The optimization was done in two steps. First, the molecular mechanics' force field 3 (MM3) and the output were optimized using the semi-empirical parameterization method 6 (PM6). After that, infra-red spectra were calculated to ensure system reliability using PM6 in water method (Bikadi & Hazai, 2009). Then, we also optimize the positive control compounds (O6K and N3) that we retrieved from the protein data bank (<https://www.rcsb.org/>) (PDB IDs: 6Y2G and 6LU7) (Jin et al., 2020; Sussman et al., 1998; Zhang et al., 2020). After optimization, all the ligands were prepared using AutoDock tools 1.5.6 by adding missing hydrogen atoms and charges (Kollman and Gasteiger) (Morris et al., 2009). Finally, the PDBQT files of the ligands were saved to be ready for the docking experiments.



We previously simulated the Mpro (dimer conformation) of SARS-CoV-2 (PDB ID: 6Y2G) for 100 ns to study its dynamics. After that, we clustered the trajectories into five groups. We utilized representative cluster conformations in this study to test ligand binding affinities (A. M. Elgohary et al., 2022). The docking was performed using the five representative conformations to overcome the bias exerted by the rigid x-ray structure.

## **2.2 Molecular Docking (MDocking)**

The five representative conformations were prepared using AutoDock Tools 1.5.6 software, where missed H-atoms were added, but water and cofactors were removed. The docking was performed using AutoDock Vina 1.2.2 (Trott & Olson, 2010) The active site (H41 and C145) was treated as flexible during the docking (Jin et al., 2020). Ligands were also treated as flexible in the docking protocol, where the rotamers were detected by AutoDock Tools 1.5.6 during the preparation stage. The docking box was set to cover the active site residues H41 and C145, having a size of  $30 \times 30 \times 30 \text{ \AA}^3$ .

## **2.3 Molecular Dynamics (MD) Simulations**

MD simulations of the best two compounds-Mpro and a positive control N3-Mpro complexes, were performed by the GROMACS software utilizing the CHARMM36 force field. The input files were generated using the Charmm GUI webserver (Lee et al., 2016). The simulation lasted for 150 ns using the TIP3P water model at 1 atm pressure and 310 K temperature. The systems were ionized with NaCl of concentration 0.154 M (Harrach & Drossel, 2014; Mark & Nilsson, 2001). A cubic periodic boundary condition simulation box was utilized during the run at the NVT ensemble (Phillips et al., 2005).

Simulation trajectories were then analyzed using VMD 1.9.3 software and some in-house codes (Humphrey et al., 1996; Pettersen et al., 2004). Furthermore, the Molecular Mechanics-Generalized Born Surface Area (MM-GBSA) was calculated for the complexes using Amber tools to deconvolute the binding affinity as a per-residue contribution and the binding energy contributions (Genheden & Ryde, 2015; Miller et al., 2012).

## **2.4 *In-silico* Prediction of Physicochemical Properties, Pharmacokinetic and Toxicity Profiles**

The physicochemical properties, pharmacokinetic and toxicity profiles of the fourteen laulimalide-containing macrolides (**1-14**) in our screening library (**Scheme 1**) were calculated using the pkCSM online webtool

(<http://biosig.unimelb.edu.au/pkcsml/prediction>, accessed on 24 March 2023) (Pires et al., 2015).

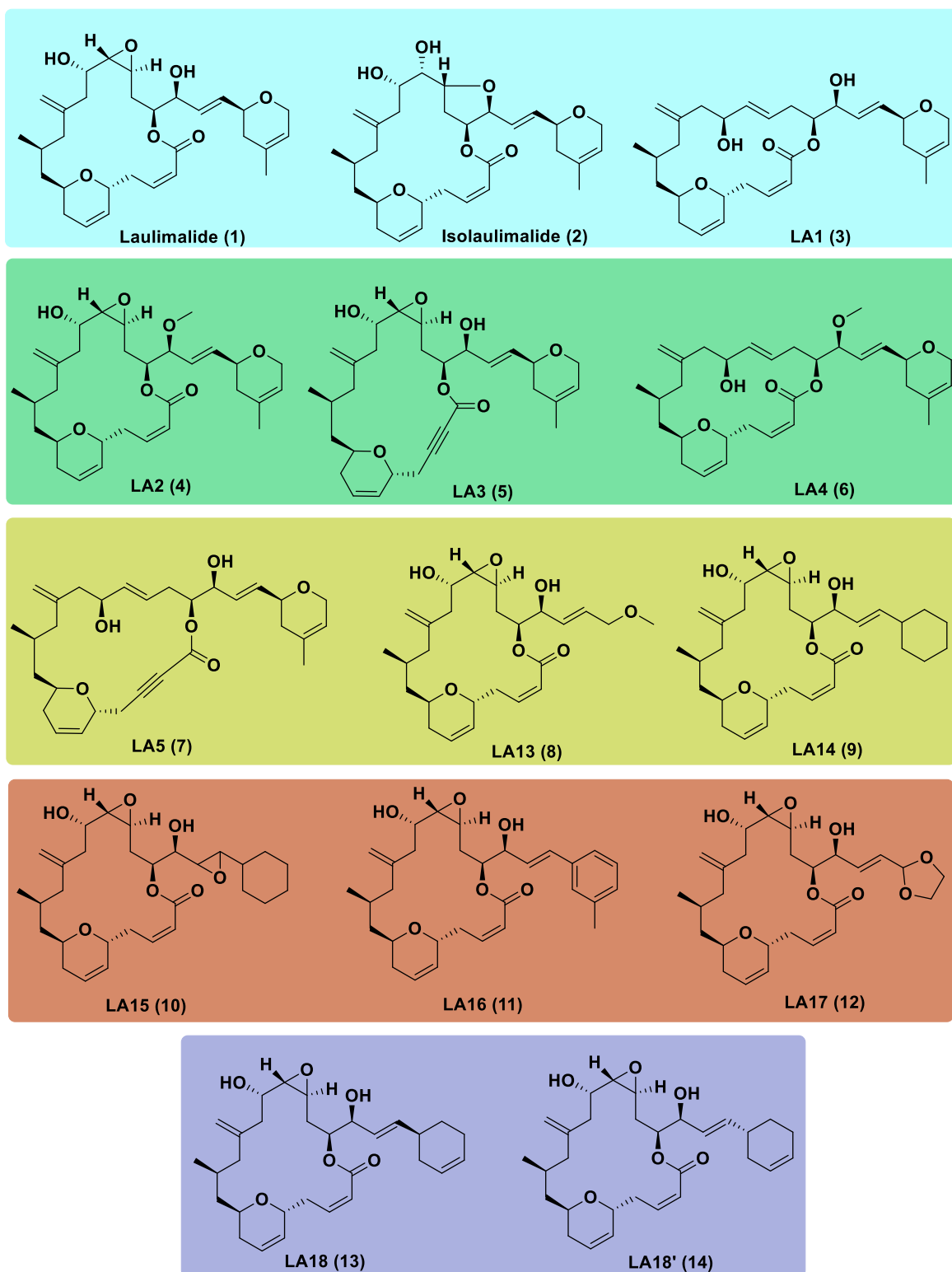
The pkCSM tool comprises six physicochemical properties, such as molecular weight (MW), octanol–water partition coefficient (LogP), number of rotatable bonds, number of hydrogen bond donors, number of hydrogen bond acceptors, and surface area. The pharmacokinetic profile of a compound defines its absorption, distribution, metabolism, and excretion (ADME) properties.

The pkCSM tool has currently available seven absorption properties (water solubility, Caco-2 permeability, intestinal absorption (human), skin permeability, P-glycoprotein substrate, P-glycoprotein I inhibitor, P-glycoprotein II inhibitor), four distribution properties (VDss (human), fraction unbound (human), BBB (blood-brain barrier) permeability, CNS (central nervous system) permeability), seven metabolism properties (CYP2D6 substrate, CYP3A4 substrate, CYP1A2 inhibitor, CYP2C19 inhibitor, CYP2C9 inhibitor, CYP2D6 inhibitor, CYP3A4 inhibitor), and two excretion properties (total clearance, renal OCT2 substrate).

The potential toxicity profiles of these compounds were predicted using the pkCSM, which has eight available properties: AMES toxicity, maximum tolerated dose (human), oral rat acute toxicity (LD50), oral rat chronic toxicity (LOAEL), hERG I inhibitor, hERG II inhibitor, hepatotoxicity, and skin sensitization (Baell & Holloway, 2010; Daina et al., 2017).

## **2.5. Identification of laulimalides Marine Macrolides**

A focused list of naturally occurring and synthetic homologues of fourteen laulimalides marine-containing macrolides (**1-14**) were selected and demonstrated as in (**Scheme 1**). Comprehensive details about their isolations, structural characterizations and synthetic preparations, were previously reported by Clark *et al.*, (Clark et al., 2006) and Mooberry *et al.*, (Mooberry et al., 2004; Mooberry et al., 1999).



**Scheme 1.** Chemical structure of laulimalides (1-14)

### 3. Results and Discussions

#### 3.1 Molecular Docking and Binding Energies Studies

In the current study, a focused list of fourteen laulimalides marine-containing macrolides (**scheme 1**) were *in-silico* investigated against SARS-CoV-2 Mpro, aiming to evaluate their binding energies and binding mode to the active site of Mpro. As previously reported, the 100 ns MDS of the Apo-Mpro was enough to equilibrate the protein system at the NVT ensemble (Alaa M. Elgohary et al., 2022). The root-mean-square fluctuations also ensured system stability during the simulation, so we used the structural conformations in the current study. Additionally, this trajectory was redocked with the positive control **O6K** and was successful with root-mean-square displacement  $< 1.0 \text{ \AA}$ . **Figure 1** shows the average binding energies (in Kcal/mol) for the ligands (**O6K**, **N3**, and the 14 laulimalides marine macrolides) to the Mpro active site (H41 and C145). Error bars represent the standard deviation of the mean.

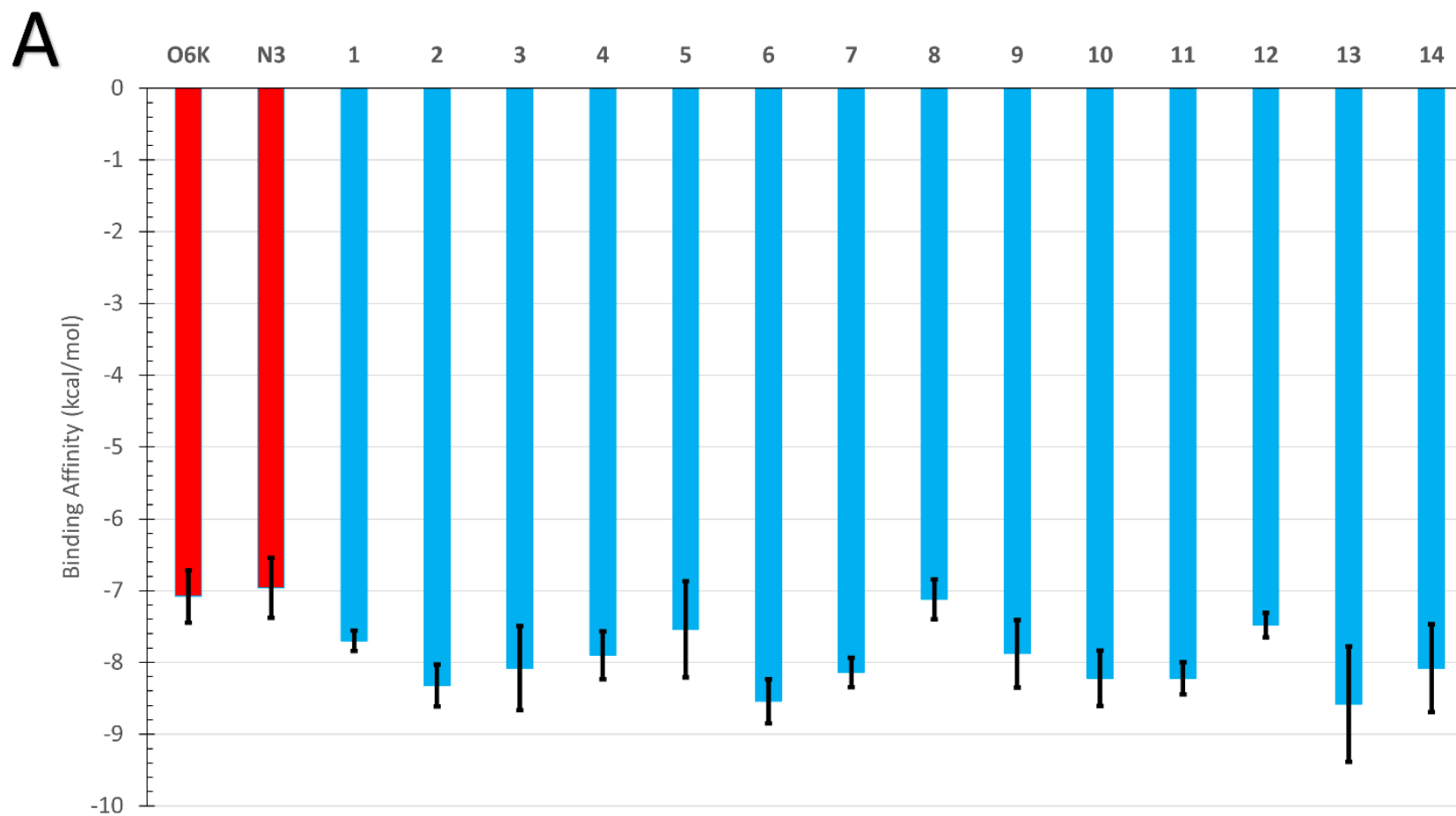


**Figure 1 (A):** The docking of the laulimalides compounds (**1-14**) to the SARS-CoV-2 Mpro. (A) The average binding energies calculated using AutoDock Vina software for the five different conformations with error bars represent the standard deviation.

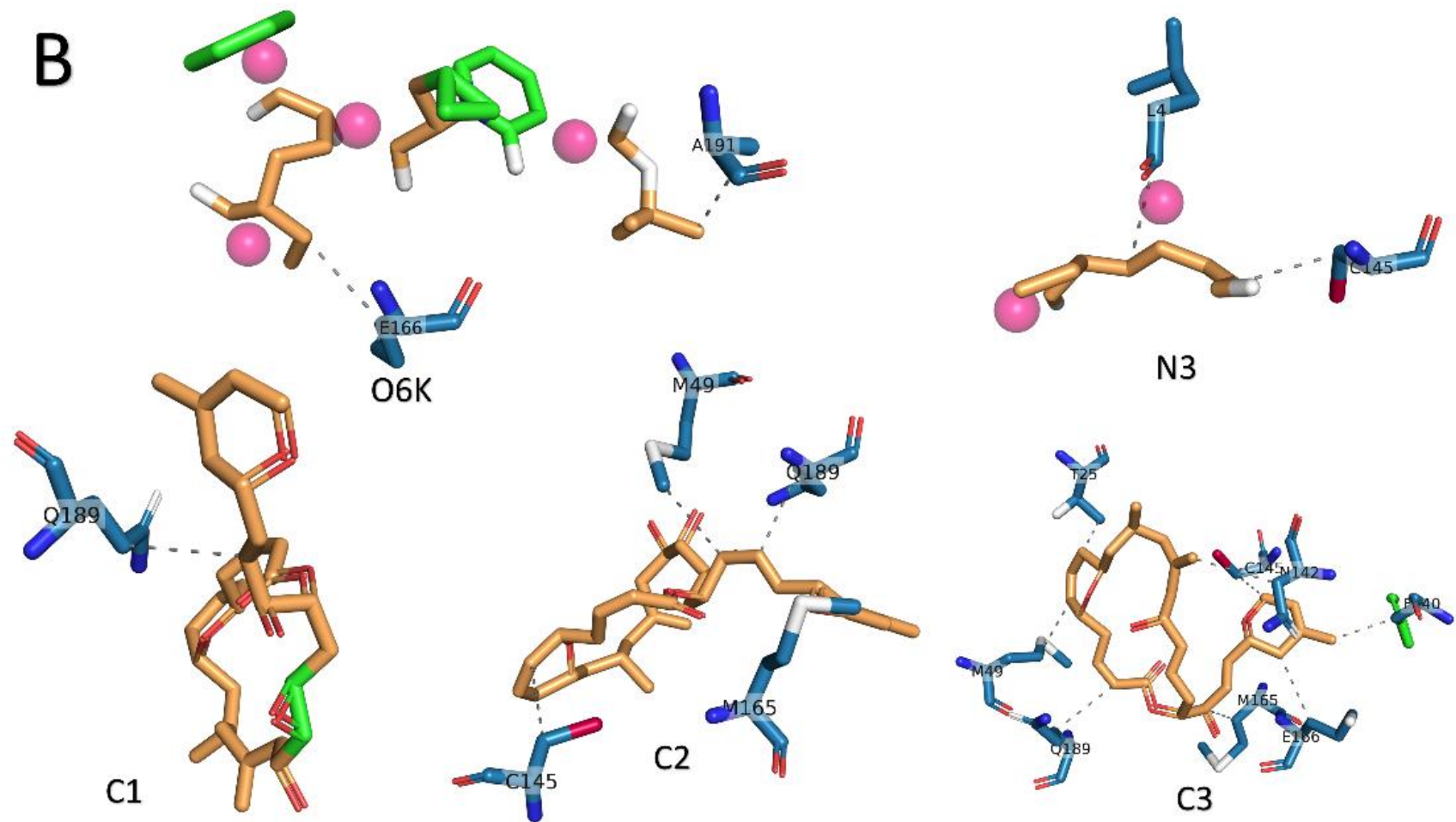
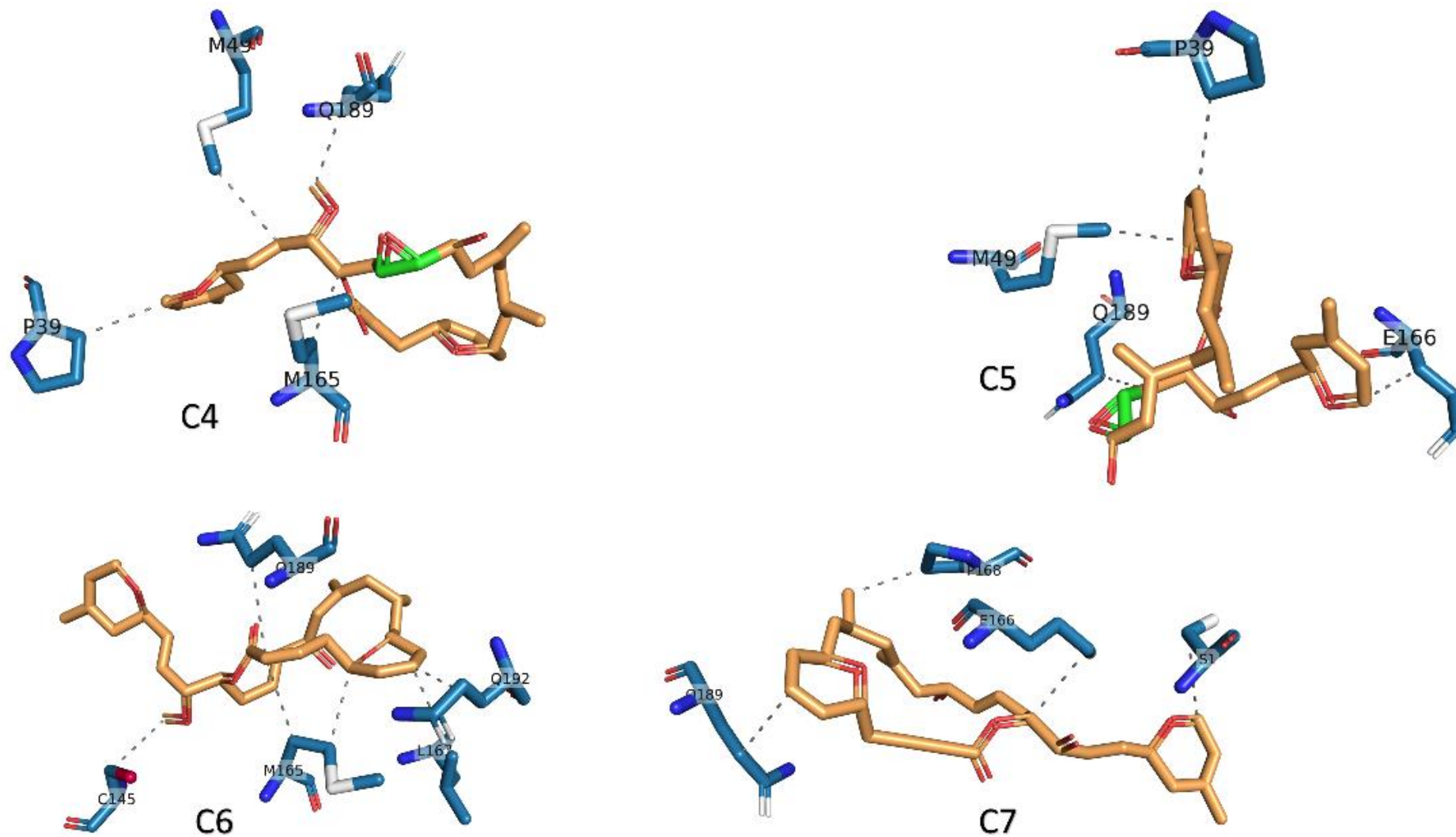
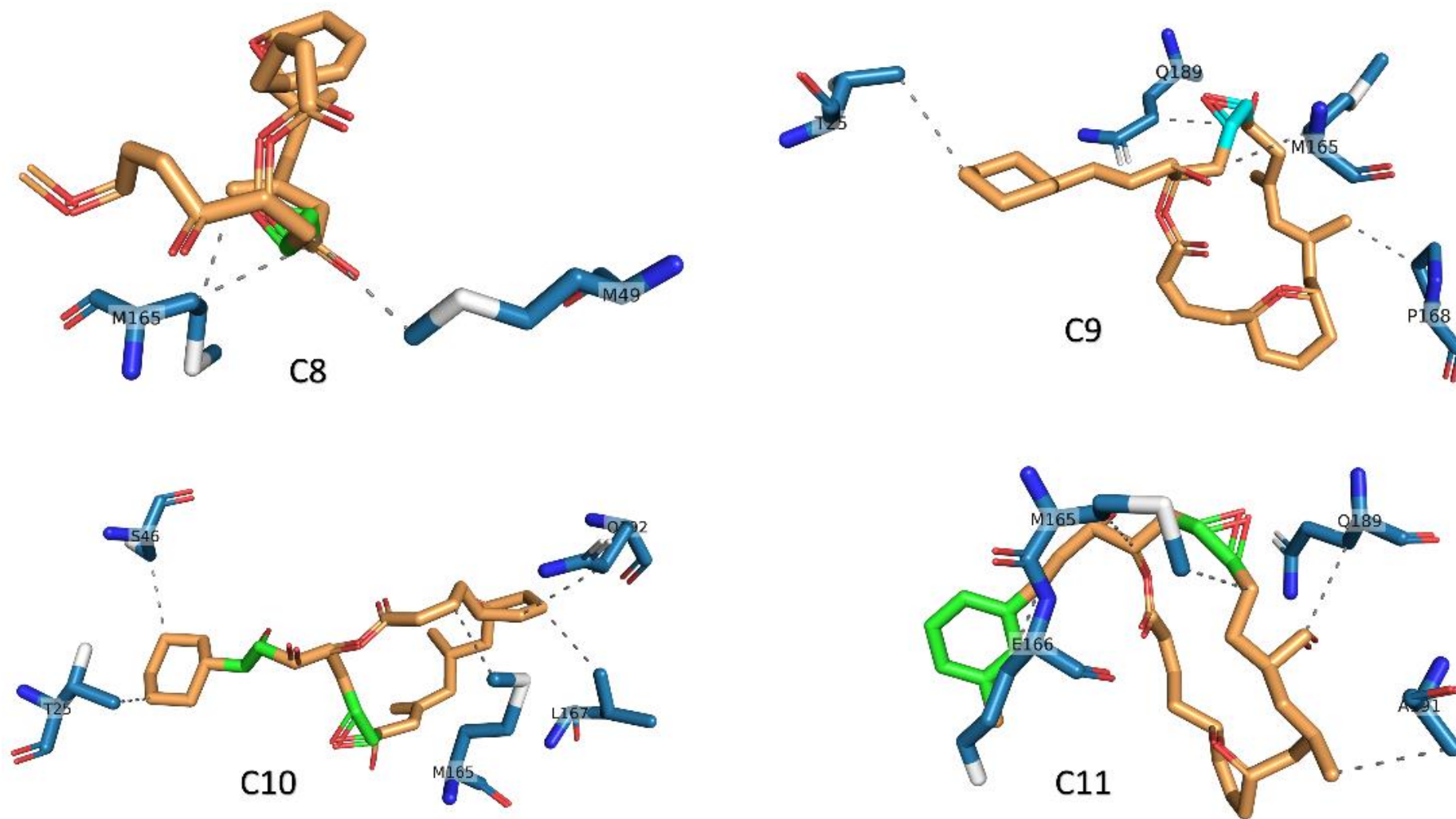


**Figure 1 (B):** The docking poses (compounds **1-3**) selected for each ligand against the two positive controls, **N3** and **OK6** (the closest to the average binding affinity value) are predicted by the PLIP web server and drawn by PyMOL. Blue lines and dashed-gray lines represent the formed H-bonds and hydrophobic contacts.

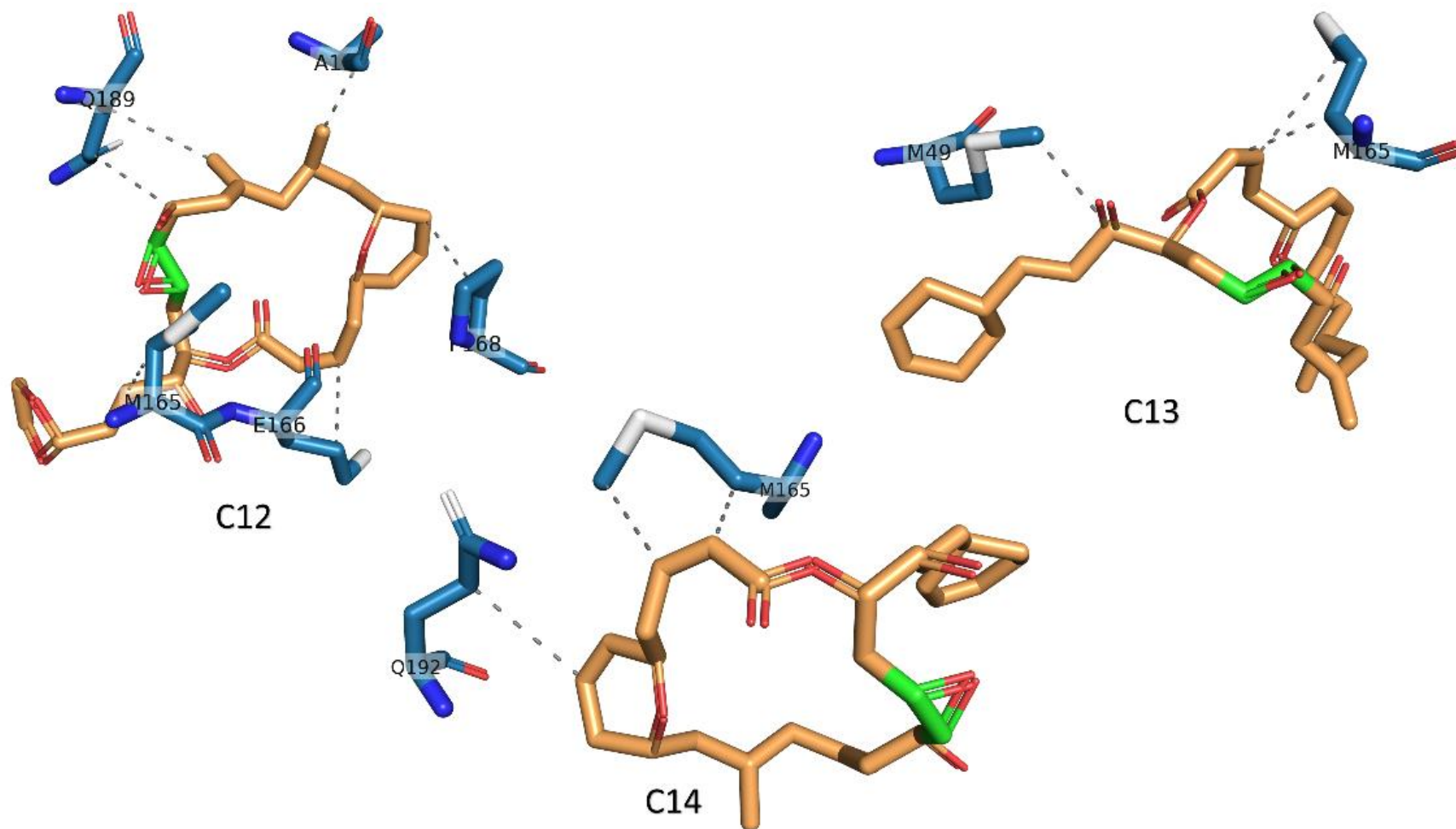


Continued **Figure 1 (B)**: The docking poses (compounds 4-7) against the two positive control N3 and OK6



Continued **Figure 1 (B)**: The docking poses (compounds **8-11**) against the two positive control **N3** and **OK6**





*Continued Figure 1 (B):* The docking poses (compounds **12-14**) against the two positive control **N3** and **OK6**

Most compounds demonstrated lower average binding energies (more negative values) compared to the positive control (**O6K** and **N3**). Particularly, the two compounds, laulimalides LA4 (**6**) and LA18 (**13**), showed the best binding affinities to the Mpro active site with average binding energies of  $-8.54 \pm 0.31$  and  $-8.58 \pm 0.80$  Kcal/mol, respectively.

**Table 1** and **Figure 1 (B)** summarize the formed interactions established upon docking. Most docking experiments establish two types of interactions: H-bonds and hydrophobic contacts. For the 14 compounds, the average number of formed H-bonds is 2.14, while the average number of established hydrophobic contacts is 4.57. This reflects the importance of the hydrophobic contacts in binding the ligands at the Mpro active site. This coincides with our previous findings with marine polycyclic batzelladine alkaloids that we suggested as promising inhibitors for Mpro (Alaa M. Elgohary et al., 2022).

Additionally, the hydrophobic contacts were more critical than H-bonds in Mpro binding of novel bis-[1,3,4]thiadiazolimines and bis-Thiazolimines (Gomha et al., 2022).

For the best two compounds [laulimalides LA4 (**6**) and LA18 (**13**)], six hydrophobic contacts and at least one H-bond have been displayed between the ligand and the Mpro residues. The most reported residues to form hydrophobic contacts are M165, Q189, E166, M49, and C145, with the detected occurrence of 15, 13, 8, 6, and 5, respectively, while the residues H164 and Q189 (5 events each) form H-bonds upon docking.

**Table 1:** The detailed interactions established upon docking the **O6K**, **N3**, and marine macrolides (1-14) against the SARS-CoV-2 Mpro (PDB ID: 6Y2G, Chain A) retrieved from PLIP webserver and visualized by PyMOL. Bold residues are the active site dyads H41 and C145.

| Ligand     | Binding affinity (kcal/mol) | Hydrophobic Interactions |  | H-bonds |                        |
|------------|-----------------------------|--------------------------|--|---------|------------------------|
|            |                             | No.                      | Residues involved  | No.     | Residues involved      |
| <b>O6K</b> | $-7.08 \pm 0.37$            | 2                        | E166 and A191  | -       | -                      |
| <b>N3</b>  | $-6.96 \pm 0.42$            | 2                        | L4 and <b>C145</b>                                       | 3       | N142, G143, and S301   |
| <b>1</b>   | $-7.70 \pm 0.14$            | 1                        | Q189   | 2       | G143 and <b>C145</b>   |
| <b>2</b>   | $-8.32 \pm 0.29$            | 4                        | M49, <b>C145</b> , M165, and Q189                        | 3       | <b>H41</b> and Q189(2) |
| <b>3</b>   | $-8.08 \pm 0.58$            | 8                        | T25, M49, F140, N142, <b>C145</b> , M165, E166, and Q189 | 1       | E166                   |
| <b>4</b>   | $-7.90 \pm 0.34$            | 4                        | P39, M49, M165, and Q189                                 | 3       | H164 and Q192(2)       |

|           |                       |   |   |   |                                    |
|-----------|-----------------------|---|---|---|------------------------------------|
| <b>5</b>  | -7.54<br>±0.67        | 4 | P39, M49, E166, and Q189                    | 1 | Q189                               |
| <b>6</b>  | <b>-8.54</b><br>±0.31 | 6 | <b>C145</b> , M165(2), L167, Q189, and Q192 | 1 | H164                               |
| <b>7</b>  | -8.14<br>±0.21        | 4 | S1, E166, P168, and Q189                    | 2 | S1* and N142                       |
| <b>8</b>  | -7.12<br>±0.28        | 3 | M49 and M165(2)                             | 5 | H163, H164, E166, R188, and Q189   |
| <b>9</b>  | -7.88<br>±0.47        | 4 | T25, M165, P168, and Q189                   | 2 | H164 and T190                      |
| <b>10</b> | -8.22<br>±0.39        | 5 | T25, S46, M165, L167, and Q192              | - | -                                  |
| <b>11</b> | -8.22<br>±0.22        | 6 | M165(2), E166(2), Q189, and A191            | 2 | <b>H41</b> and Q189                |
| <b>12</b> | -7.48<br>±0.17        | 6 | M165, E166, P168, Q189(2), and A191         | 3 | G143, S144, and <b>C145</b>        |
| <b>13</b> | <b>-8.58</b><br>±0.80 | 6 | M49, <b>C145</b> , M165, E166, and Q189(2)  | 4 | G143, <b>C145</b> , H164, and E166 |
| <b>14</b> | -8.08<br>±0.61        | 3 | M165(2) and Q192                            | 1 | N142                               |

\* The interaction occurred between the compound and Chain B of the Mpro.

The best two chemical hints [laulimalides LA4 (**6**) and LA18 (**13**)] complexed with Mpro are subjected to a 150 ns MDS run to quantify their binding energies further. Additionally, the complex of N3-Mpro was also simulated for comparison.

### 3.2 Molecular Dynamic simulations (MDS)

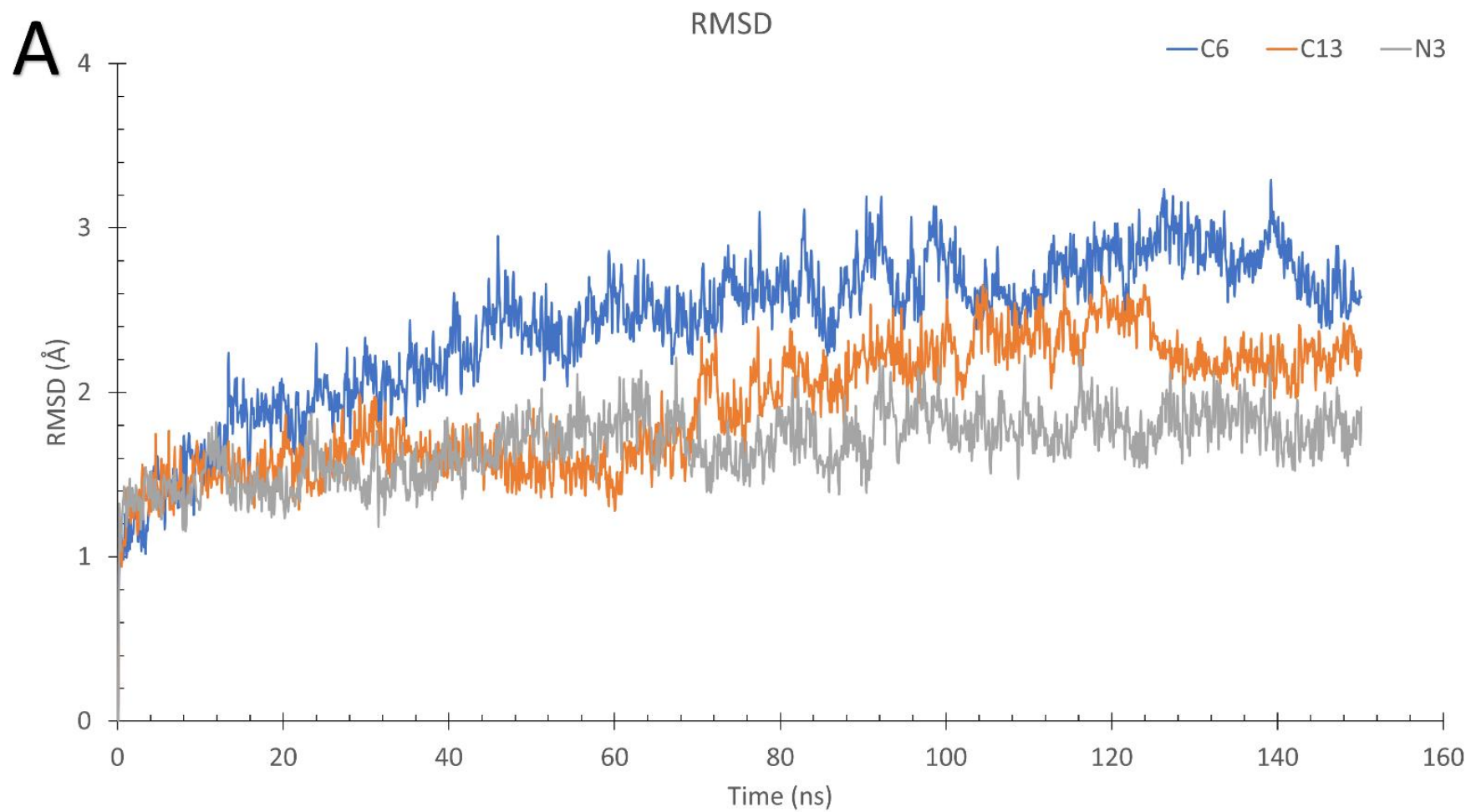
**Figure 2** shows MDS analysis where the protein backbone root-mean-square deviation (RMSD) in Å (A), ligand-RMSD in Å (B), the radius of gyration (RoG) in Å (C), surface accessible surface area (SASA) in nm<sup>2</sup> (D), the number of total H-bonds (E), and the protein-ligand H-bonds (F) are plotted against the simulation time in ns. Additionally, the per-residue root-mean-square fluctuations (RMSF) in Å for Chain A (upper) and Chain B (lower) are plotted in **Figure 2G**. The **N3**, laulimalide LA4 (**6**), and laulimalide LA18 (**13**) are shown in gray, blue, and orange lines in **Figure 2**.

All three systems were equilibrated after 60 ns (around 2 Å) with a slight elevation of the RMSD values for laulimalide LA4 (**6**), and laulimalide LA18 (**13**) (2.2 and 2.0 Å) compared to the positive control **N3** (1.6 Å). On the other hand, the ligand-RMSD exhibits the opposite pattern, where the positive control **N3** shows slightly higher values (4.0 Å) compared to laulimalide LA4 (**6**) (2.8 Å) and laulimalide LA18 (**13**) (1.8 Å). The three systems are stable during the simulation, as reflected by the RoG, SASA, and the total number of H-bonds (protein backbone) in **Figures 2C-2E**.

The curves coincide and fluctuate around 26.1 Å, 270 nm<sup>2</sup>, and 440 for the RoG, SASA, and total H-bonds, respectively. The protein-ligand H-bonds also reflect systems stability during the simulation as the number of H-bonds fluctuates between 1 and 3 in most frames of the three trajectories. RMSF in **Figure 2G** of the Mpro complexes with [**N3** (gray), laulimalides LA4 (**6**) (blue), and LA18 (**13**) (orange)] for chain A (upper) and chain B (lower) show identical behavior previously reported with other complexes (Adem et al., 2022).

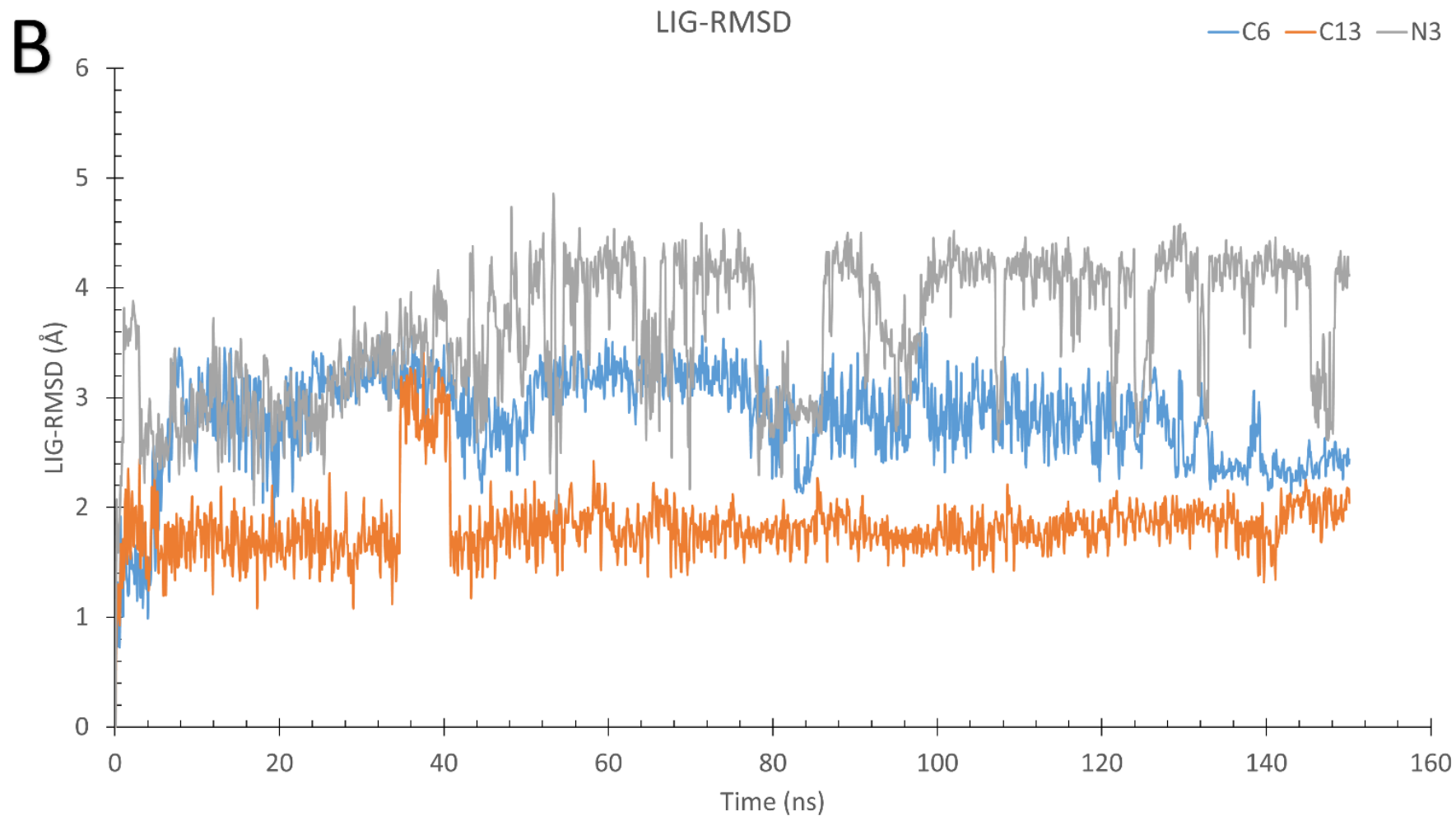
Only one region of moderate fluctuations was reported for residues centered around 48, reflecting the flexibility of the loop I43-P52. Additionally, the protein terminals are flexible, but other regions show low fluctuations in all the complexes (RMSF < 3 Å).

The MM-GBSA calculated for the binding energies of the positive control N3 (gray), [laulimalides LA4 (**6**) (blue), and LA18 (**13**) (orange)] to Mpro is shown in **Figure 2H**. The error bars represent the standard deviation for each value. The average binding energies of laulimalide LA4 (**6**) (-9.91 ±8.1 Kcal/mol) did not significantly differ from the positive control **N3**. On the other hand, laulimalide LA18 (**13**) 's average binding energy value (-20.51 ±6.1 Kcal/mol) is lower than that of the positive control (-16.31 ±8.5 Kcal/mol). This reflects the potential of the laulimalide LA18 (**13**) to bind to and hence inhibit Mpro, which is yet to be verified experimentally.

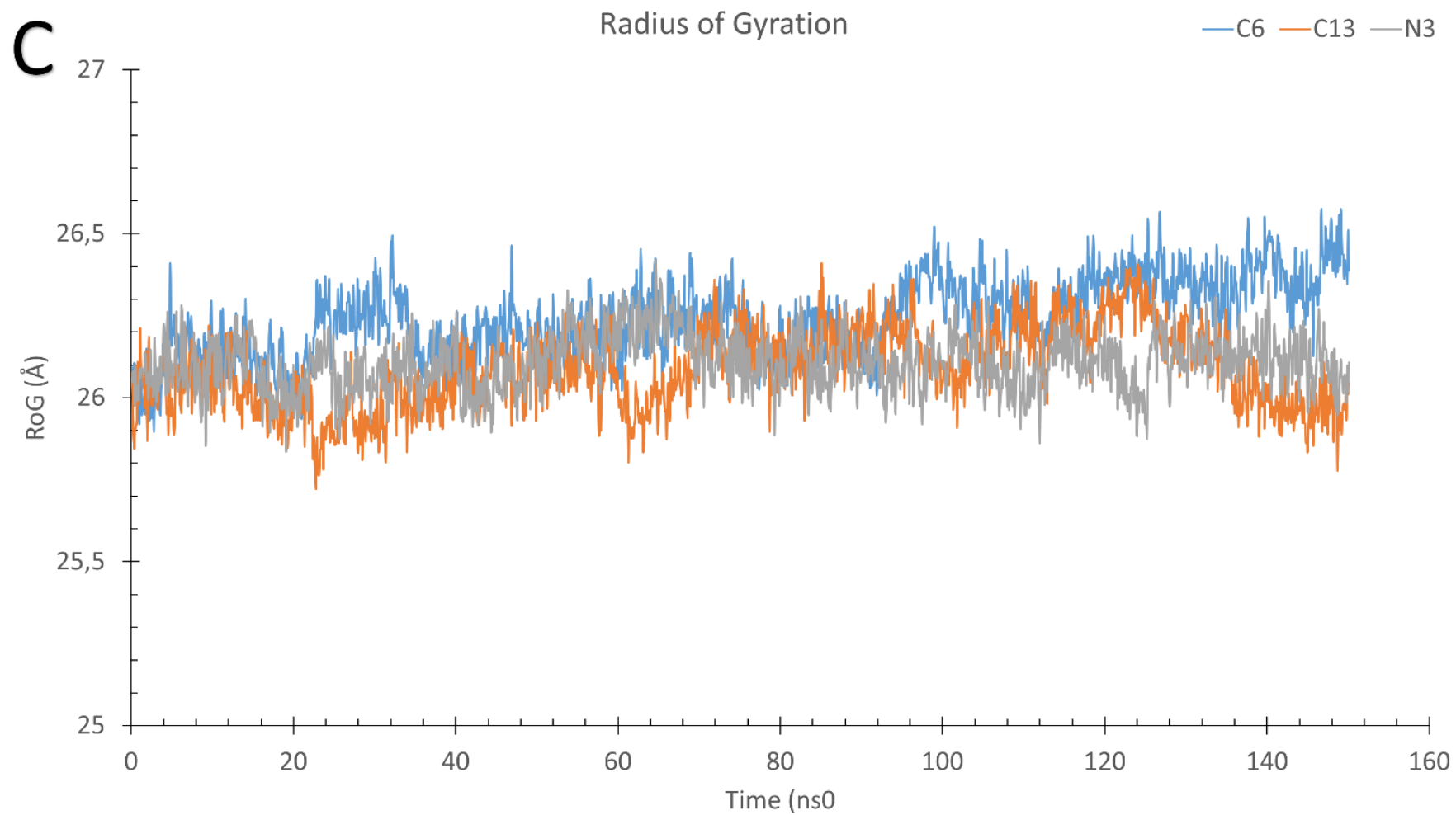


Molecular Dynamics Simulation trajectory analysis for the complexes of Mpro with **N3** (gray), laulimalides LA4 (**6**) (blue), and LA18 (**13**) (orange).

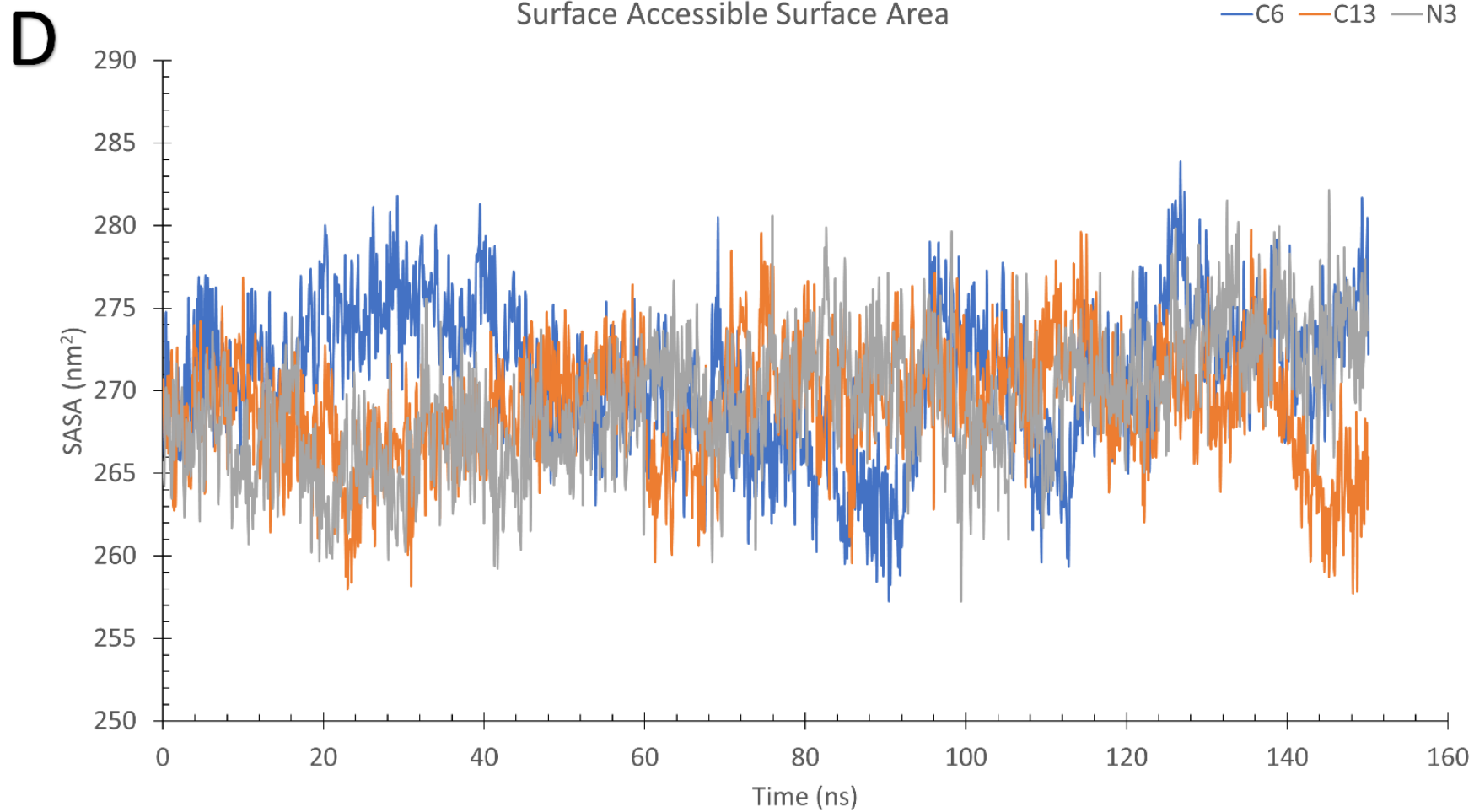
**Figure 2A:** The protein backbone Root-mean-square deviation (RMSD) in Å.



*Continued:* Molecular Dynamics Simulation trajectory analysis for the complexes of Mpro with N3 (gray), laulimalides LA4 (**6**) (blue), and LA18 (**13**) (orange). **Figure 3B:** The ligand-protein RMSD in Å.

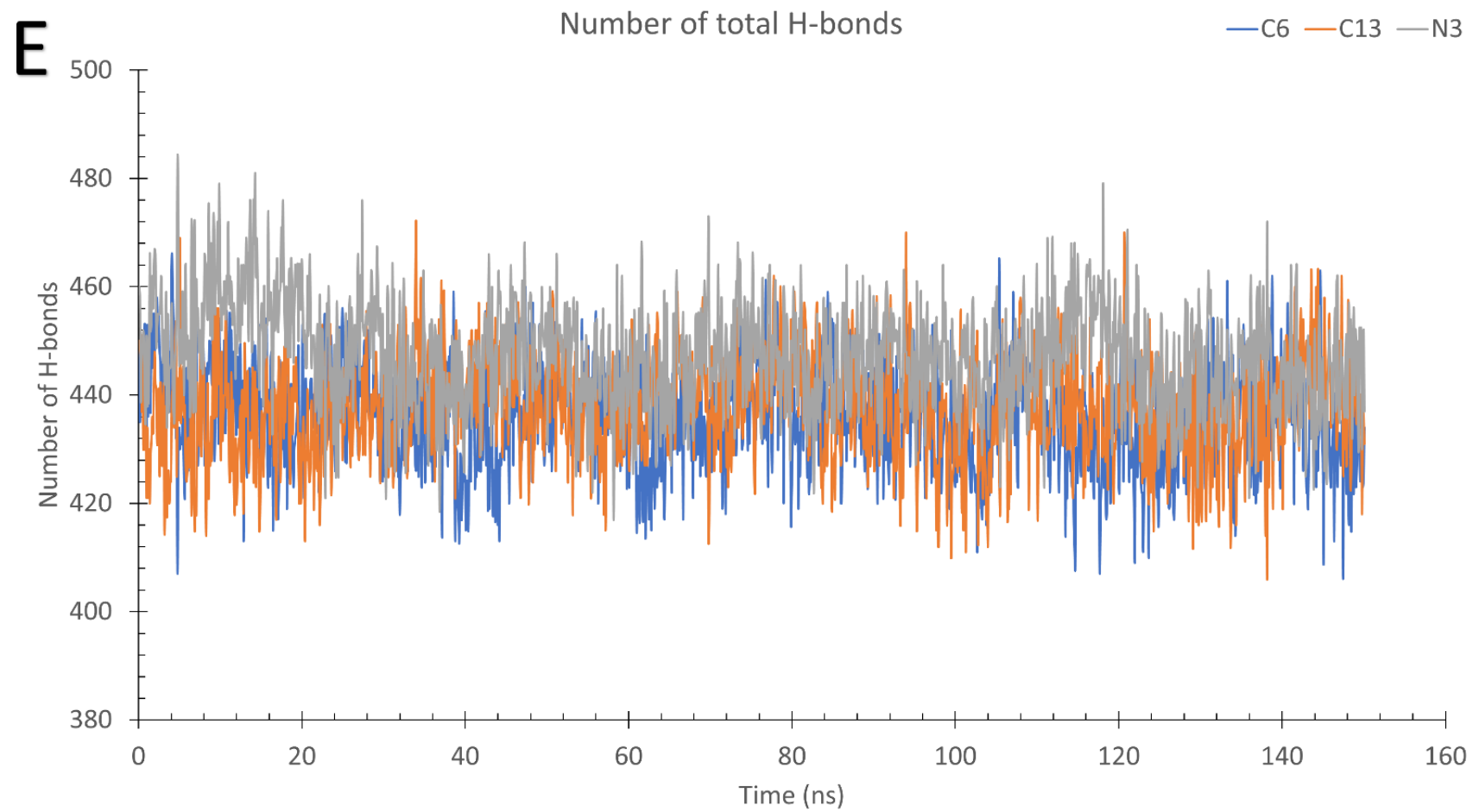


*Continued:* Molecular Dynamics Simulation trajectory analysis for the complexes of Mpro with **N3** (gray), laulimalides LA4 (**6**) (blue), and LA18 (**13**) (orange). **Figure 4C:** The Radius of Gyration (RoG) in Å.

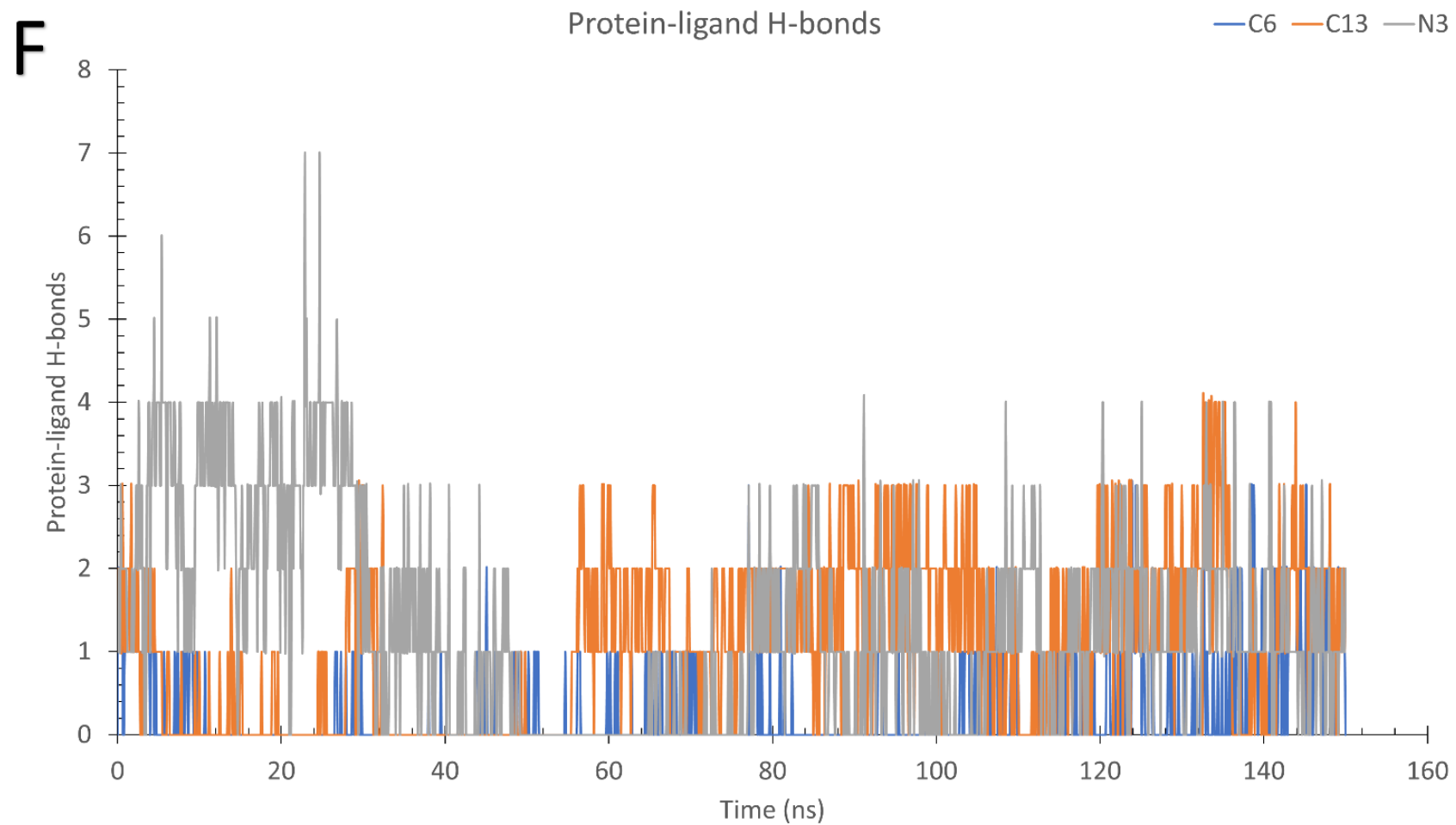


*Continued:* Molecular Dynamics Simulation trajectory analysis for the complexes of Mpro with N3 (gray), laulimalides LA4 (**6**) (blue), and LA18 (**13**) (orange). **Figure 5D:** Surface Accessible Surface Area (SASA) in nm<sup>2</sup>.

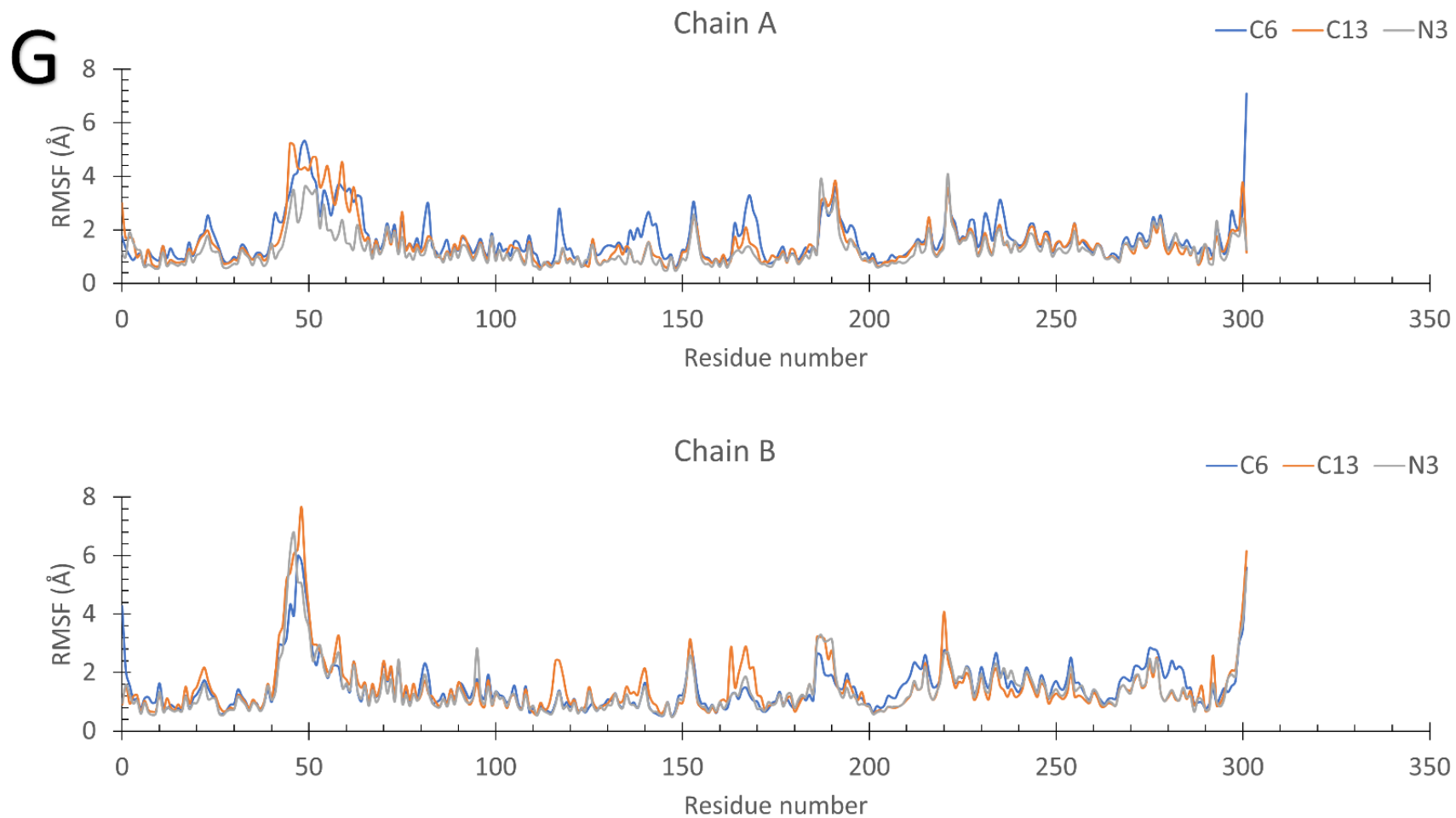




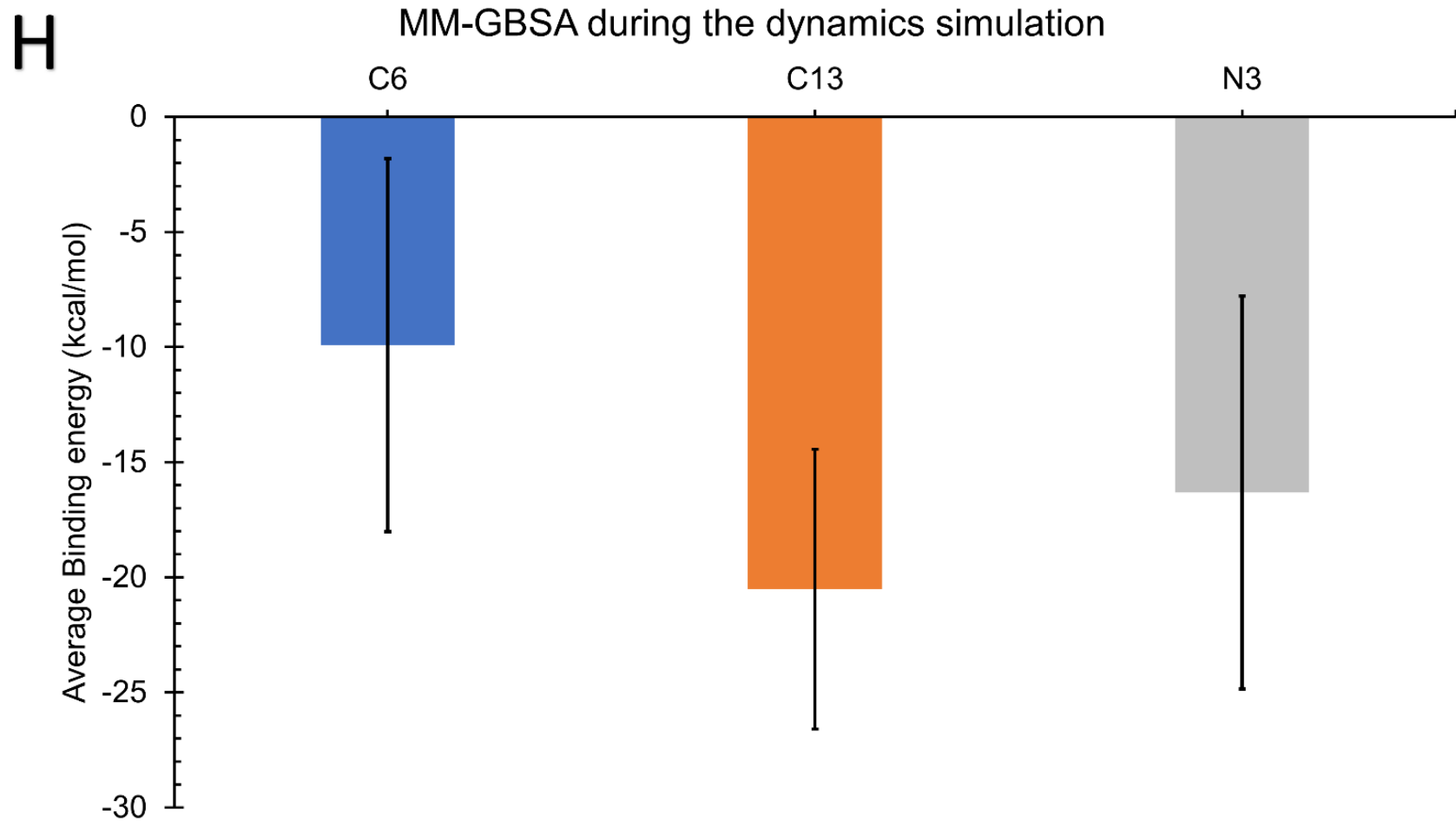
*Continued:* Molecular Dynamics Simulation trajectory analysis for the complexes of Mpro with N3 (gray), laulimalides LA4 (**6**) (blue), and LA18 (**13**) (orange). **Figure 6E:** The number of total H-bonds.



*Continued:* Molecular Dynamics Simulation trajectory analysis for the complexes of Mpro with N3 (gray), laulimalides LA4 (**6**) (blue), and LA18 (**13**) (orange). **Figure 7F:** The protein-ligand H-bonds, versus the simulation time in ns.



*Continued:* Molecular Dynamics Simulation trajectory analysis for the complexes of Mpro with **N3** (gray), laulimalides LA4 (**6**) (blue), and LA18 (**13**) (orange). **Figure 8G:** The per-residue root-mean-square fluctuations (RMSF) in Å for the two chains of the dimeric Mpro.



*Continued:* Molecular Dynamics Simulation trajectory analysis for the complexes of Mpro with **N3** (gray), laulimalides LA4 (**6**) (blue), and LA18 (**13**) (orange). **Figure 9H:** The calculated MM-GBSA for the three complexes after the dynamics in kcal/mol. Error bars represent the standard deviation.

#### 4. Structure activity Relationships (SARs)

All fourteen investigated laulimalide-containing macrolides (**1-14**), shown in (Scheme 1), share a common 20-membered structure containing eight chiral centers (5*R*, 9*S*, 11*S*, 15*S*, 16*S*, 17*S*, 19*S*, 20*S*) highlighted in blue, as shown in (Figure 3), and with predicted free binding energies ( $\Delta G_B$ ) ranging from -8.58 Kcal/mol to -7.12 Kcal/mol (Table 1). Seven of them possess the core structure of laulimalide (**1**) only changing the C-23 side chain (**8-9,11-14**), between a methoxy group in LA13 (**8**), a cyclohexane ring in LA14 (**9**), a phenyl ring in LA16 (**11**), a dioxolane ring in LA17 (**12**) and a cyclohexene ring in LA18 (**13**) and LA19 (**14**), as shown in Figure 4.1, with predicted  $\Delta G_B$  between -8.58 and -7.12 Kcal/mol (Table 1). Derivatives LA18 (**13**) and LA19 (**14**) are diastereoisomers, differing only in the configuration of the C-23 chiral center, 23*S* in LA18 (**13**) like laulimalide (**1**) and 23*R* in LA19 (**14**), with predicted  $\Delta G_B$  of -8.58 and -8.08 Kcal/mol, respectively.

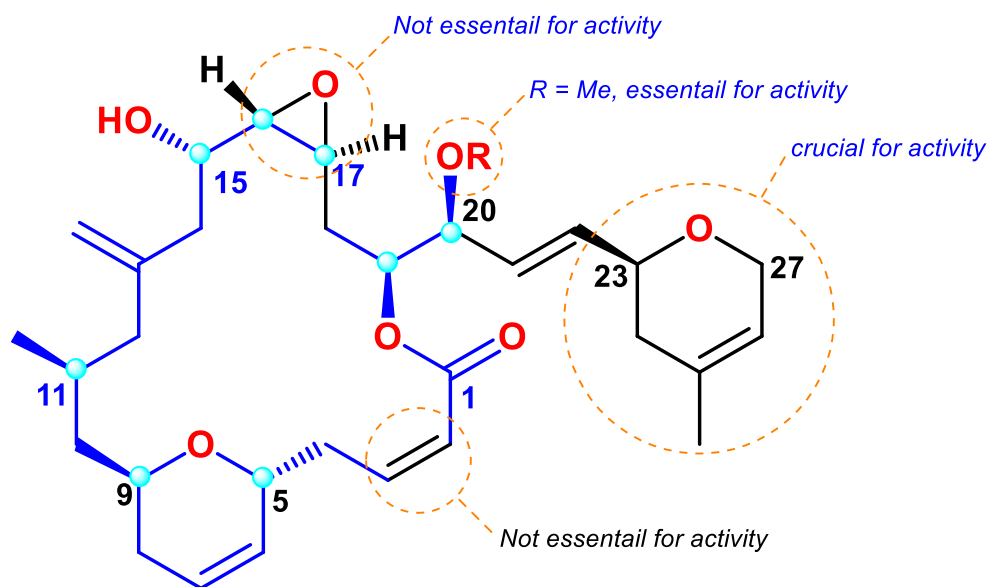


**Figure 3.** Common structural core with numeration of laulimalides

In LA2 (**4**), only the substituent at position C-20 has changed from a hydroxyl group in laulimalide (**1**) to a methoxyl group in LA2 (**4**), with a predicted  $\Delta G_B$  of -7.90 Kcal/mol. There are three derivatives (**3, 6, 7**) in which depoxidation occurs at positions C-16 and C-17, as compared to laulimalide (**1**): LA3 (**3**) has the same substitution pattern as laulimalide (**1**), LA4 (**6**) has a methoxy group at position 20, and LA5 (**7**) has a triple bond at positions 2 and 3, with predicted free binding energies of -8.08, -8.54, and -8.14 Kcal/mol, respectively.

Finally, isolaulimalide (**2**) is an isomer of laulimalide (**1**), the tetrahydrofuran ring of which is formed by an S<sub>N</sub>2-type attack of the C-20 hydroxygroup at the C-17 position of the epoxide in laulimalide (**1**), with a predicted  $\Delta G_B$  of -8.32 Kcal/mol, compared with -7.70 Kcal/mol for laulimalide (**1**). In the same way as has been reported for anti-cancer activity (Cao et al., 2018), the lack of the epoxide moiety at the C-16 and C-17 positions in isolaulimalide (**2**) and LA1 (**3**) does not translate into an increase in the predicted  $\Delta G_B$ , which suggests that the epoxide moiety of laulimalide may not be an essential feature for the activity against SARS-CoV-2 Mpro. As can be seen by the  $\Delta G_B$  calculated values for the isolaulimalide (**2**) and LA1 (**3**) of -8.32 Kcal/mol and -8.08 Kcal/mol (**Table 1**), respectively, compared to -7.70 Kcal/mol for laulimalide (**1**).

The substitution of the C-20 hydroxyl group with the C-20 methoxyl group appears to favor the activity against SARS-CoV-2 Mpro, as can be seen in a decrease in the  $\Delta G_B$  calculated in the C-20 methoxylated derivatives LA2 (**4**) and LA4 (**6**) of -7.9 and -8.54 Kcal/mol, respectively, when compared to the C-20 hydroxylated derivatives laulimalide (**1**) and LA1 (**3**) of -7.7 and -8.08 Kcal/mol, respectively. The substitution of the 2,3-Z-double bond for a triple bond in the derivatives LA3 (**5**) and LA5 (**7**) with  $\Delta G_B$  values of -7.54 and -8.14 Kcal/mol, respectively, does not result in a significant variation of the predicted  $\Delta G_B$  when compared to the corresponding derivatives with the double bond, laulimalide (**1**) and LA1 (**3**), with  $\Delta G_B$  values of -7.7 and -8.08 Kcal/mol, respectively.

The C-23 side chain (derivatives **8-9, 11-14**) appears to be very relevant for the activity against SARS-CoV-2 Mpro in accordance with previously reported anti-cancer activity (Cao et al., 2018; Morris et al., 2022). The structural variation in the C-23 side chain includes: (I) oxygen-containing substituents such as dihydropyran (**1**), methoxy (**8**) and 1,3-dioxalane (**12**) with calculated  $\Delta G_B$  of -7.7, -7.12 and -7.48 Kcal/mol, respectively; (II) carbon 6-membered rings such as cyclohexane (**9**), phenyl (**11**) and cyclohexene (**13** and **14**) with calculated  $\Delta G_B$  of -7.88, -8.22, -8.58 and -8.08 Kcal/mol, respectively. The C-23 configuration also appears to be extremely important for activity, as can be seen in the  $\Delta G_B$  calculated for epimers LA18 (**13**) and LA19 (**14**) of -8.58 and -8.08 Kcal/mol, respectively. Epoxidation of the *trans*-21,22 double bond also translates into a decrease in the calculated  $\Delta G_B$  value of -8.22 Kcal/mol for LA15 (**10**) compared to -7.88 Kcal/mol for LA14 (**9**).

## 5. Druglikeness and Pharmacokinetics

To evaluate the druglikeness behaviour of the fourteen investigated laulimalide-containing macrolides (**1-14**), the Lipinski's Rule of five was applied based on the physicochemical properties predicted by the pkCSM tool. It is observed that only the derivative LA4 (**6**) fails two of the four Lipinski's rules (MW and LogP). There are seven derivatives that fail one of the Lipinski's rules (MW): laulimalide (**1**), isolaulimalide (**2**), LA2 (**4**), LA3 (**5**), LA14 (**9**), LA15 (**10**) and LA16 (**11**). The remaining six derivatives do not fail any of the Lipinski's rules. All laulimalide-containing macrolides were predicted with an adequate pharmacokinetic profile taking into account the ADME properties. Considering the toxicological prediction profile, only hepatotoxicity issues were raised for nine derivatives including laulimalide (**1**), isolaulimalide (**2**), LA1 (**3**), LA3 (**5**), LA4 (**6**), LA5 (**7**), LA16 (**11**), LA18 (**13**) and LA19 (**14**).

## 6. Conclusions

An integrated array of computational tools comprising MDock, MD and SARs studies were manipulated for investigating the binding affinities of a total of 14 laulimalide-containing marine macrolides (**LMM**) against the SARS-CoV-2 main protease (Mpro) dimer. Interestingly, the molecular docking and binding energy studies demonstrated promising binding capabilities of the different laulimalide ligands with average binding energies less than that demonstrated by the positive controls, [**O6K** and **N3**]. Best binding affinities to the Mpro active site were manifested by the laulimalides, LA4 (**6**) and LA18 (**13**), that showed average binding energies less than 8 Kcal/mol. Moreover, stable molecular dynamics within the accommodated (Mpro) pockets were demonstrated by the most potent laulimalides, LA4 (**6**) and LA18 (**13**).

For linking the chemical structure of the assessed laulimalides with the generated suggested activity, a preliminary structure activity relationship study was performed. Results demonstrated the crucial role of the C-23 side chain in influencing the activity against SARS-CoV-2 Mpro. Besides, the C-20 methoxyl group proved to enhance the laulimalide activity. Druglikeness and pharmacokinetics studies assured the adequate physicochemical and pharmacokinetic profiles of the evaluated laulimalides with some attributes with the hepatotoxicity of certain derivatives. In conclusion, the evaluated set of laulimalide derivatives could be regarded as promising leads for combating the COVID-19. Further *in vitro* and *in vivo* assays are highly recommended for better

investigation of the promising activities of laulimalide derivatives, in particular for LA4 (6) and LA18 (13) prior proceeding to clinical trials.

#### **Authorship contribution statement**

**Conceptualization:** Abdo A. Elfiky and Amr El-Demerdash. **Validation:** Abdo A. Elfiky, Amr El-Demerdash. **Formal analysis:** Abdo A. Elfiky, Alaa M. Elgohary, Florbela Pereira, and Amr El-Demerdash. **Investigation:** Abdo A. Elfiky, Alaa M. Elgohary, Florbela Pereira and Amr El-Demerdash. **Resources:** Abdo A. Elfiky, Alaa M. Elgohary, Florbela Pereira, Mariam I. Gamal El-Din, Mohamed. A. Tammam, Mohamed Sebak and Amr El-Demerdash. **Data curation:** Abdo A. Elfiky, Alaa M. Elgohary, Florbela Pereira and Amr El-Demerdash. **Writing original draft:** Abdo A. Elfiky, Alaa M. Elgohary, Florbela Pereira, Mariam I. Gamla El-Din, Mohamed. A. Tammam, Mohamed Sebak, Sherif Hamdallah, Emad Shehata and Amr El-Demerdash. **Writing-review & editing:** Abdo A. Elfiky, Alaa M. Elgohary, Florbela Pereira, Mariam I. Gamla El-Din, Mohamed. A. Tammam, Mohamed Sebak, Sherif Hamdallah, Emad Shehata and Amr El-Demerdash.

#### **Declaration of competing interest**

The authors declare that they have no known competing financial interests or personal relationships that could have appeared to influence the work reported in this paper.

#### **Funding**

Amr El-Demerdash is immensely grateful to the John Innes Centre, Norwich Research Park, United Kingdom for the postdoctoral fellowship. Florbela Pereira would like to thank Fundação para a Ciência e a Tecnologia, MCTES, in the scope of the project UIDB/50006/2020 of the Research Unit, Associate Laboratory for Green Chemistry, LAQV".

#### **Acknowledgments**

We thank ChemAxon Ltd. for access to JChem and Marvin. Bibliotheca Alexandrina's high-performance computing facility (Bib Alex) was utilized for the MD simulations. Mr. Jameel Abdeljalil is thankful for his assistance with the MD simulations.



## References

- Adem, Ş., Eyupoglu, V., Ibrahim, I. M., Sarfraz, I., Rasul, A., Ali, M., & Elfiky, A. A. (2022). Multidimensional in silico strategy for identification of natural polyphenols-based SARS-CoV-2 main protease (Mpro) inhibitors to unveil a hope against COVID-19. *Comput Biol Med*, *145*, 105452. <https://doi.org/https://doi.org/10.1016/j.compbimed.2022.105452>
- Alimohamadi, Y., Sepandi, M., Taghdir, M., & Hosamirudsari, H. (2020). Determine the most common clinical symptoms in COVID-19 patients: a systematic review and meta-analysis. *Journal of preventive medicine and hygiene*, *61*(3), E304.
- Almutairi, F. M., Mohareb, R. M., Elfiky, A. A., Mahmoud, M. A. A., Wardakhan, W. W., Mohamed, M. S., & Abdelhameed, A. S. (2022). Synthesis, Molecular Docking, c-Met inhibitions of 2,2,2-Trichloro-ethylidene-cyclohexane-1,3-dione Derivatives Together With Their Application as Target SARS-CoV-2 main Protease (Mpro) And as Potential Anti-Covid-19. *Combinatorial chemistry & high throughput screening*. <https://doi.org/10.2174/1386207325666220829111236>
- Amr, E.-D., Ahmed, M., Metwaly, T. M., El-Aziz, A., Ibrahim, H., & Eissa, J. D. (2020). Comprehensive Virtual Screening of the Antiviral Potentialities of Marine Polycyclic Guanidine Alkaloids against SARS-CoV-2 (Covid-19)(preprint).
- Baell, J. B., & Holloway, G. A. (2010). New Substructure Filters for Removal of Pan Assay Interference Compounds (PAINS) from Screening Libraries and for Their Exclusion in Bioassays. *Journal of Medicinal Chemistry*, *53*(7), 2719-2740. <https://doi.org/10.1021/jm901137j>
- Bikadi, Z., & Hazai, E. (2009). Application of the PM6 semi-empirical method to modeling proteins enhances docking accuracy of AutoDock. *J Cheminform*, *1*(1), 15. <https://doi.org/10.1186/1758-2946-1-15>
- Cao, Y.-N., Zheng, L.-L., Wang, D., Liang, X.-X., Gao, F., & Zhou, X.-L. (2018). Recent advances in microtubule-stabilizing agents. *European Journal of Medicinal Chemistry*, *143*, 806-828.
- Carroll, A. R., Copp, B. R., Davis, R. A., Keyzers, R. A., & Prinsep, M. R. (2022). Marine natural products. *Natural product reports*, *39*(6), 1122-1171.
- Cheng, L., & Mishra, H. (2022). Why did only one genus of insects, Halobates, take to the high seas? *PLoS Biology*, *20*(4), e3001570.
- Churchill, C. D., Klobukowski, M., & Tuszynski, J. A. (2016). Analysis of the binding mode of laulimalide to microtubules: Establishing a laulimalide–tubulin pharmacophore. *Journal of Biomolecular Structure and Dynamics*, *34*(7), 1455-1469.
- Clark, E. A., Hills, P. M., Davidson, B. S., Wender, P. A., & Mooberry, S. L. (2006). Laulimalide and synthetic laulimalide analogues are synergistic with paclitaxel and 2-methoxyestradiol. *Molecular Pharmaceutics*, *3*(4), 457-467.
- Daina, A., Michielin, O., & Zoete, V. (2017). SwissADME: a free web tool to evaluate pharmacokinetics, drug-likeness and medicinal chemistry friendliness of small molecules. *Scientific Reports*, *7*(1), 42717. <https://doi.org/10.1038/srep42717>
- Das, R., Rauf, A., Mitra, S., Emran, T. B., Hossain, M. J., Khan, Z., Naz, S., Ahmad, B., Meyyazhagan, A., & Pushparaj, K. (2022). Therapeutic potential of marine macrolides: An overview from 1990 to 2022. *Chemico-Biological Interactions*, 110072.
- El-Demerdash, A., Atanasov, A. G., Horbanczuk, O. K., Tammam, M. A., Abdel-Mogib, M., Hooper, J. N., Sekeroglu, N., Al-Mourabit, A., & Kijjoa, A. (2019). Chemical diversity and biological activities of marine sponges of the genus *Suberea*: A systematic review. *Marine drugs*, *17*(2), 115.
- El-Demerdash, A., Ermolenko, L., Gros, E., Retailleau, P., Thanh, B. N., Anne, G.-B., & Al-Mourabit, A. Short-Cut Bio-Inspired Synthesis of Tricyclic Guanidinic Motifs of Crambescidins and

- Batzelladines Marine Alkaloids. *European Journal of Organic Chemistry*, n/a(n/a). <https://doi.org/10.1002/ejoc.202000744>
- El-Demerdash, A., Hassan, A., Abd El-Aziz, T. M., Stockand, J. D., & Arafa, R. K. (2021). Marine brominated tyrosine alkaloids as promising inhibitors of SARS-CoV-2. *Molecules*, 26(20), 6171.
- El-Demerdash, A., Metwaly, A. M., Hassan, A., Abd El-Aziz, T. M., Elkaeed, E. B., Eissa, I. H., Arafa, R. K., & Stockand, J. D. (2021). Comprehensive virtual screening of the antiviral potentialities of marine polycyclic guanidine alkaloids against SARS-CoV-2 (COVID-19). *Biomolecules*, 11(3), 460.
- El-Demerdash, A., Petek, S., Debitus, C., & Al-Mourabit, A. (2020). Crambescidin Acid from the French Polynesian *Monanchora* n. sp. Marine Sponge. *Chemistry of Natural Compounds*, 56(6), 1180-1182. <https://doi.org/10.1007/s10600-020-03262-1>
- El-Din, M. I. G., George, M. Y., & Youssef, F. S. (2023). Chemical characterization of the polyphenolic rich fraction of *Thunbergia erecta* and its therapeutic potential against doxorubicin and cyclophosphamide-induced cognitive impairment in rats. *Journal of ethnopharmacology*, 307, 116213.
- El-Din, M. I. G., & Youssef, F. S. Non-Food Applications of Coriander Seed Extracts. In *Handbook of Coriander (Coriandrum sativum)* (pp. 545-558). CRC Press.
- Elfiky, A. A., A., G. W., & M., E. W. (2016). Hepatitis C Viral Polymerase Inhibition using Directly Acting Antivirals, A Computational Approach. In M. A (Ed.), *Software and Techniques for Bio-Molecular Modeling* (pp. 197). Austin publishing group.
- Elfiky, A. A., Ibrahim, I. M., Ibrahim, M. N., & Elshemey, W. M. (2022). Host-cell recognition of SARS-CoV-2 spike receptor binding domain from different variants. *Journal of Infection*, 85(6), 702-769. <https://doi.org/10.1016/j.jinf.2022.10.009>
- Elgohary, A. M., Elfiky, A. A., Pereira, F., Abd El-Aziz, T. M., Sobeh, M., Arafa, R. K., & El-Demerdash, A. (2022). Investigating the structure-activity relationship of marine polycyclic batzelladine alkaloids as promising inhibitors for SARS-CoV-2 main protease (Mpro). *Computers in Biology and Medicine*, 147, 105738.
- Elgohary, A. M., Elfiky, A. A., Pereira, F., Abd El-Aziz, T. M., Sobeh, M., Arafa, R. K., & El-Demerdash, A. (2022). Investigating the structure-activity relationship of marine polycyclic batzelladine alkaloids as promising inhibitors for SARS-CoV-2 main protease (M(pro)). *Comput Biol Med*, 147, 105738. <https://doi.org/10.1016/j.compbiomed.2022.105738>
- Elgohary, A. M., Elfiky, A. A., Pereira, F., Abd El-Aziz, T. M., Sobeh, M., Arafa, R. K., & El-Demerdash, A. (2022). Investigating the structure-activity relationship of marine polycyclic batzelladine alkaloids as promising inhibitors for SARS-CoV-2 main protease (Mpro). *Comput Biol Med*, 147, 105738. <https://doi.org/https://doi.org/10.1016/j.compbiomed.2022.105738>
- Gamal El-Din, M. I., Youssef, F. S., Altyar, A. E., & Ashour, M. L. (2022). GC/MS Analyses of the essential oils obtained from different *Jatropha* species, their discrimination using chemometric analysis and assessment of their antibacterial and anti-biofilm activities. *Plants*, 11(9), 1268.
- Gamal El-Din, M. I., Youssef, F. S., Ashour, M. L., Eldahshan, O. A., & Singab, A. N. B. (2018). Comparative analysis of volatile constituents of *Pachira aquatica* Aubl. and *Pachira glabra* Pasq., their anti-Mycobacterial and anti-*Helicobacter pylori* activities and their metabolic discrimination using chemometrics. *Journal of Essential Oil Bearing Plants*, 21(6), 1550-1567.
- Genheden, S., & Ryde, U. (2015). The MM/PBSA and MM/GBSA methods to estimate ligand-binding affinities. *Expert Opin Drug Discov*, 10(5), 449-461. <https://doi.org/10.1517/17460441.2015.1032936>

- Ghareeb, M. A., Tammam, M. A., El-Demerdash, A., & Atanasov, A. G. (2020). Insights about clinically approved and Preclinically investigated marine natural products. *Current Research in Biotechnology*, 2, 88-102.
- Ghosh, A. K., & Wang, Y. (2000). Total synthesis of (-)-laulimalide. *Journal of the American Chemical Society*, 122(44), 11027-11028.
- Gollner, A., & Mulzer, J. (2008). Total synthesis of neolaulimalide and isolaulimalide. *Organic Letters*, 10(20), 4701-4704.
- Gomha, S. M., Riyadh, S. M., Abdellattif, M. H., Abolibda, T. Z., Abdel-aziz, H. M., Nayl, A. A., Elgohary, A. M., & Elfiky, A. A. (2022). Synthesis and In Silico Study of Some New bis-[1,3,4]thiadiazolimines and bis-Thiazolimines as Potential Inhibitors for SARS-CoV-2 Main Protease. *Current Issues in Molecular Biology*, 44(10), 4540-4556. <https://www.mdpi.com/1467-3045/44/10/311>
- Harrach, M. F., & Drossel, B. (2014). Structure and dynamics of TIP3P, TIP4P, and TIP5P water near smooth and atomistic walls of different hydroaffinity. *J Chem Phys*, 140(17), 174501. <https://doi.org/10.1063/1.4872239>
- Hassan, S. S., Aljabali, A. A., Panda, P. K., Ghosh, S., Attrish, D., Choudhury, P. P., Seyran, M., Pizzol, D., Adadi, P., & Abd El-Aziz, T. M. (2021). A unique view of SARS-CoV-2 through the lens of ORF8 protein. *Computers in Biology and Medicine*, 133, 104380.
- Humphrey, W., Dalke, A., & Schulten, K. (1996). VMD: visual molecular dynamics. *J Mol Graph*, 14(1), 33-38, 27-38. [https://doi.org/10.1016/0263-7855\(96\)00018-5](https://doi.org/10.1016/0263-7855(96)00018-5)
- Ibrahim, I. M., Elfiky, A. A., Fathy, M. M., Mahmoud, S. H., & ElHefnawi, M. (2022). Targeting SARS-CoV-2 endoribonuclease: a structure-based virtual screening supported by in vitro analysis. *Scientific reports*, 12(1), 13337. <https://doi.org/10.1038/s41598-022-17573-6>
- Jin, Z., Du, X., Xu, Y., Deng, Y., Liu, M., Zhao, Y., Zhang, B., Li, X., Zhang, L., Peng, C., Duan, Y., Yu, J., Wang, L., Yang, K., Liu, F., Jiang, R., Yang, X., You, T., Liu, X., . . . Yang, H. (2020). Structure of Mpro from SARS-CoV-2 and discovery of its inhibitors. *Nature*, 582(7811), 289-293. <https://doi.org/10.1038/s41586-020-2223-y>
- Lee, J., Cheng, X., Swails, J. M., Yeom, M. S., Eastman, P. K., Lemkul, J. A., Wei, S., Buckner, J., Jeong, J. C., Qi, Y., Jo, S., Pande, V. S., Case, D. A., Brooks, C. L., 3rd, MacKerell, A. D., Jr., Klauda, J. B., & Im, W. (2016). CHARMM-GUI Input Generator for NAMD, GROMACS, AMBER, OpenMM, and CHARMM/OpenMM Simulations Using the CHARMM36 Additive Force Field. *J Chem Theory Comput*, 12(1), 405-413. <https://doi.org/10.1021/acs.jctc.5b00935>
- Liu, J., Towle, M. J., Cheng, H., Saxton, P., Reardon, C., Wu, J., Murphy, E. A., Kuznetsov, G., Johannes, C. W., & Tremblay, M. R. (2007). In vitro and in vivo anticancer activities of synthetic (-)-laulimalide, a marine natural product microtubule stabilizing agent. *Anticancer research*, 27(3B), 1509-1518.
- Ma, H.-G., Liu, Q., Zhu, G.-L., Liu, H.-S., & Zhu, W.-M. (2016). Marine natural products sourced from marine-derived Penicillium fungi. *Journal of asian natural Products research*, 18(1), 92-115.
- Mark, P., & Nilsson, L. (2001). Structure and dynamics of the TIP3P, SPC, and SPC/E water models at 298 K. *The Journal of Physical Chemistry A*, 105(43), 9954-9960.
- Miller, B. R., 3rd, McGee, T. D., Jr., Swails, J. M., Homeyer, N., Gohlke, H., & Roitberg, A. E. (2012). MMPBSA.py: An Efficient Program for End-State Free Energy Calculations. *J Chem Theory Comput*, 8(9), 3314-3321. <https://doi.org/10.1021/ct300418h>
- Mooberry, S. L., Randall-Hlubek, D. A., Leal, R. M., Hegde, S. G., Hubbard, R. D., Zhang, L., & Wender, P. A. (2004). Microtubule-stabilizing agents based on designed laulimalide analogues. *Proceedings of the National Academy of Sciences*, 101(23), 8803-8808.
- Mooberry, S. L., Tien, G., Hernandez, A. H., Plubrukarn, A., & Davidson, B. S. (1999). Laulimalide and isolaulimalide, new paclitaxel-like microtubule-stabilizing agents. *Cancer Research*, 59(3), 653-660.

- Moriou, C., Lacroix, D., Petek, S., El-Demerdash, A., Trepos, R., Leu, T. M., Florean, C., Diederich, M., Hellio, C., Debitus, C., & Al-Mourabit, A. (2021). Bioactive Bromotyrosine Derivatives from the Pacific Marine Sponge *Suberea clavata* (Pulitzer-Finali, 1982). *Marine Drugs*, 19(3), 143. <https://www.mdpi.com/1660-3397/19/3/143>
- Morris, G. M., Huey, R., Lindstrom, W., Sanner, M. F., Belew, R. K., Goodsell, D. S., & Olson, A. J. (2009). AutoDock4 and AutoDockTools4: Automated docking with selective receptor flexibility. *J Comput Chem*, 30(16), 2785-2791. <https://doi.org/10.1002/jcc.21256>
- Morris, J. D., Takahashi-Ruiz, L., Persi, L. N., Summers, J. C., McCauley, E. P., Chan, P. Y., Amberchan, G., Lizama-Chamu, I., Coppage, D. A., & Crews, P. (2022). Re-evaluation of the Fijianolide/Laulimalide Chemotype Suggests an Alternate Mechanism of Action for C-15/C-20 Analogs. *ACS Omega*, 7(10), 8824-8832.
- Mulzer, J., & Öhler, E. (2003). Microtubule-stabilizing marine metabolite laulimalide and its derivatives: synthetic approaches and antitumor activity. *Chemical reviews*, 103(9), 3753-3786.
- Ng, T. I., Correia, I., Seagal, J., DeGoey, D. A., Schrimpf, M. R., Hardee, D. J., Noey, E. L., & Kati, W. M. (2022). Antiviral drug discovery for the treatment of COVID-19 infections. *Viruses*, 14(5), 961.
- Pan, Y., Wang, L., Feng, Z., Xu, H., Li, F., Shen, Y., Zhang, D., Liu, W. J., Gao, G. F., & Wang, Q. (2023). Characterisation of SARS-CoV-2 variants in Beijing during 2022: an epidemiological and phylogenetic analysis. *The lancet*.
- Paterson, I., De Savi, C., & Tudge, M. (2001). Total synthesis of the microtubule-stabilizing agent (-)-laulimalide. *Organic Letters*, 3(20), 3149-3152.
- Pereira, F., Bedda, L., Tammam, M. A., Alabdullah, A. K., Arafa, R. K., & El-Demerdash, A. (2022). Investigating the Antiviral Therapeutic Potentialities of Marine Polycyclic Lamellarin Pyrrole Alkaloids as Promising Inhibitors for SARS-CoV-2 and Zika Main Proteases (Mpro).
- Pettersen, E. F., Goddard, T. D., Huang, C. C., Couch, G. S., Greenblatt, D. M., Meng, E. C., & Ferrin, T. E. (2004). UCSF Chimera—a visualization system for exploratory research and analysis. *Journal of Computational Chemistry*, 25(13), 1605-1612.
- Phillips, J. C., Braun, R., Wang, W., Gumbart, J., Tajkhorshid, E., Villa, E., Chipot, C., Skeel, R. D., Kale, L., & Schulten, K. (2005). Scalable molecular dynamics with NAMD. *J Comput Chem*, 26(16), 1781-1802. <https://doi.org/10.1002/jcc.20289>
- Pires, D. E. V., Blundell, T. L., & Ascher, D. B. (2015). pkCSM: Predicting Small-Molecule Pharmacokinetic and Toxicity Properties Using Graph-Based Signatures. *Journal of Medicinal Chemistry*, 58(9), 4066-4072. <https://doi.org/10.1021/acs.jmedchem.5b00104>
- Qi, Y., & Ma, S. (2011). The medicinal potential of promising marine macrolides with anticancer activity. *ChemMedChem*, 6(3), 399-409.
- Romano, J. D., & Tatonetti, N. P. (2019). Informatics and computational methods in natural product drug discovery: a review and perspectives. *Frontiers in genetics*, 10, 368.
- Summers, K. L., Mahrok, A. K., Dryden, M. D., & Stillman, M. J. (2012). Structural properties of metal-free apometallothioneins. *Biochem Biophys Res Commun*, 425(2), 485-492. <https://doi.org/10.1016/j.bbrc.2012.07.141>
- Sussman, J. L., Lin, D., Jiang, J., Manning, N. O., Prilusky, J., Ritter, O., & Abola, E. E. (1998). Protein Data Bank (PDB): database of three-dimensional structural information of biological macromolecules. *Acta Crystallogr D Biol Crystallogr*, 54(Pt 6 Pt 1), 1078-1084. <https://doi.org/10.1107/s0907444998009378>
- Tammam, M. A., El-Din, M. I. G., Abood, A., & El-Demerdash, A. (2023). Recent Advances in Discovery, Biosynthesis and Therapeutic Potentialities of Isocoumarins Derived from Fungi: A Comprehensive Update. *RSC advances*, 13, 8049 - 8089.

- Tan, S. T., Kwan, A. T., Rodríguez-Barraquer, I., Singer, B. J., Park, H. J., Lewnard, J. A., Sears, D., & Lo, N. C. (2023). Infectiousness of SARS-CoV-2 breakthrough infections and reinfections during the Omicron wave. *Nature Medicine*, 1-8.
- Trott, O., & Olson, A. J. (2010). AutoDock Vina: improving the speed and accuracy of docking with a new scoring function, efficient optimization, and multithreading. *J Comput Chem*, 31(2), 455-461. <https://doi.org/10.1002/jcc.21334>
- Uzma, F., Mohan, C. D., Siddaiah, C. N., & Chowdappa, S. (2019). Endophytic fungi: promising source of novel bioactive compounds. *Advances in endophytic fungal research: present status and future challenges*, 243-265.
- W.H.O. (2023). <https://covid19.who.int/WHO> . *Coronavirus (COVID-19) Dashboard* <https://doi.org/https://covid19.who.int/>
- Wender, P. A., Hegde, S. G., Hubbard, R. D., Zhang, L., & Mooberry, S. L. (2003). Synthesis and biological evaluation of (-)-laulimalide analogues. *Organic Letters*, 5(19), 3507-3509.
- Wender, P. A., Verma, V. A., Paxton, T. J., & Pillow, T. H. (2008). Function-oriented synthesis, step economy, and drug design. *Accounts of chemical research*, 41(1), 40-49.
- Zhang, H., Zou, J., Yan, X., Chen, J., Cao, X., Wu, J., Liu, Y., & Wang, T. (2021). Marine-derived macrolides 1990–2020: An overview of chemical and biological diversity. *Marine drugs*, 19(4), 180.
- Zhang, L., Lin, D., Sun, X., Curth, U., Drosten, C., Sauerhering, L., Becker, S., Rox, K., & Hilgenfeld, R. (2020). Crystal structure of SARS-CoV-2 main protease provides a basis for design of improved  $\beta$ -ketoamide inhibitors. *SCIENCE*, 368(6489), 409-412. <https://doi.org/doi:10.1126/science.abb3405>
- Zheng, R., Xu, Y., Wang, W., Ning, G., & Bi, Y. (2020). Spatial transmission of COVID-19 via public and private transportation in China. *Travel medicine and infectious disease*, 34, 101626.
- Zhou, Y., Zhi, H., & Teng, Y. (2023). The outbreak of SARS-CoV-2 Omicron lineages, immune escape, and vaccine effectivity. *Journal of Medical Virology*, 95(1), e28138.